scientific reports

Check for updates

OPEN

Potential upscaling protocol establishment and wound healing bioactivity screening of exosomes isolated from canine adipose-derived mesenchymal stem cells

Yudith Violetta Pamulang[1,2,3], Saranyou Oontawee[2,3], Watchareewan Rodprasert[2,3], Irma Padeta[1,2,3], Noppadol Sa-Ard-lam[4,5], Rangsini Mahanonda[4,5], Thanaphum Osathanon[6,7], Poorichaya Somparn[8], Trairak Pisitkun[8], Chutirat Torsahakul[2,3,9] & Chenphop Sawangmake[2,3,10]✉

Mesenchymal stem cell-derived exosomes exhibit promising potential in tissue regeneration. Recent studies highlight its significant therapeutic potential in various stages of wound healing. However, the clinical translation of exosome-based therapy was hindered due to issues regarding low productivity and the lack of efficient production protocol to obtain a clinically relevant exosome quantity. Therefore, this study established a potential upscaling protocol to produce exosomes derived from canine adipose-derived mesenchymal stem cells (cAD-MSCs) and explored its potential for wound treatment. The potential upscaling protocol, termed VSCBIC-3-3D, was carried out using VSCBIC-3 in-house serum-free exosome-collecting solution in a three-dimensional (3D) culture system followed by the tangential flow filtration (TFF) isolation. Our findings suggest that culturing cAD-MSCs with VSCBIC-3 maintained cell morphology and viability. Compared to conventional two-dimensional (2D) protocols, The potential upscaling protocol increased exosome yield and concentration in conditioned medium by 2.4-fold and 3.2-fold, respectively. The quality assessment revealed enhanced purity and bioactivity of exosomes produced using the VSCBIC-3-3D protocol. In addition, the cAD-MSCs-derived exosomes were shown to significantly improve fibroblast migration, proliferation, and wound healing-related gene expression in vitro. This study collectively demonstrates that potential upscaling protocol establishment allowed robust production of exosomes from cAD-MSCs, which exhibit therapeutic potential for wound healing in vitro.

Keywords Exosomes, Wound healing, Upscaling production, Canine adipose-derived mesenchymal stem cells

The wound-healing process is a complex overlapping cascade, involving the interaction of the extracellular matrix (ECM) and numerous cell populations dominating each phase, which are regulated to restore the skin barrier[1,2]. Nevertheless, the normal healing process may be impeded by case-specific factors, resulting in chronic

[1]The International Graduate Program of Veterinary Science and Technology (VST), Faculty of Veterinary Science, Chulalongkorn University, Bangkok 10330, Thailand. [2]Center of Excellence for Veterinary Clinical Stem Cells and Bioengineering, Chulalongkorn University, Bangkok 10330, Thailand. [3]Veterinary Stem Cell and Bioengineering Innovation Center (VSCBIC), Faculty of Veterinary Science, Chulalongkorn University, Bangkok 10330, Thailand. [4]Immunology Research Center, Faculty of Dentistry, Chulalongkorn University, Bangkok 10330, Thailand. [5]Center of Excellence in Periodontal Disease and Dental Implant, Chulalongkorn University, Bangkok 10330, Thailand. [6]Dental Stem Cell Biology Research Unit, Department of Anatomy, Faculty of Dentistry, Chulalongkorn University, Bangkok 10330, Thailand. [7]Center of Excellence in Regenerative Dentistry, Faculty of Dentistry, Chulalongkorn University, Bangkok 10330, Thailand. [8]Center of Excellence in Systems Biology, Faculty of Medicine, Chulalongkorn University, Bangkok 10330, Thailand. [9]Department of Veterinary Medicine, Faculty of Veterinary Science, Chulalongkorn University, Bangkok 10330, Thailand. [10]Department of Pharmacology, Faculty of Veterinary Science, Chulalongkorn University, Bangkok 10330, Thailand. ✉email: chenphop.s@chula.ac.th; chenphop@gmail.com

wound healing characterized by a prolonged inflammation stage[3]. This requires increasing medical attention to complete the healing process and further omits the perpetuation of tissue damage and scar progression[4]. Regenerative treatment based on stem cells has received much attention by far since stem cell-based therapy particularly mesenchymal stem cells (MSCs) has shown therapeutic effects in various stages of the wound-healing process[2]. It is currently understood that the wound-healing properties of MSCs are not mainly generated from the proliferation and differentiation of the stem cell into dermal resident cells, in fact, the differentiation of MSCs into specific cells within the injury site is considered low and inadequate. Instead, the paracrine activity of MSCs has played a pivotal role in tissue regeneration[5,6].

Paracrine properties of MSCs are related to numerous factors including exosomes, which govern intercellular communication. The exosomes are one of the sub-populations of extracellular vesicles (EVs), which exhibit the therapeutic effect on the targeted cells through carrying cargoes of bioactive molecules namely, nucleic acid, lipids, and proteins. Several studies have reported the application of MSC-derived exosomes in altering wound healing mechanisms in nearly all stages of wound healing including promoting fibroblast migration and proliferation[7], immunomodulation activity by promoting macrophage polarization toward anti-inflammatory M2 phenotype[8], and inducing angiogenic activity[3]. In human medicine, exosomes isolated from MSCs have been intensively investigated and reported to exhibit therapeutic effects similar to MSCs themselves. However, the use of extracellular vesicles especially exosomes in veterinary study is still developing.

Regardless of its enormous therapeutic potential, the usage of exosomes isolated from MSCs has been hindered by the challenge of low productivity. In order to achieve the desired therapeutic outcome in preclinical trials, typically requires 10^9-10^{10} particles or 10–200 μg of exosomal protein per mouse[9]. However, the yield of exosomal protein from 1 mL of conditioned medium is generally less than 1 μg, indicating that collecting and purifying litters of conditioned medium is required to produce sufficient amounts of exosomes. This process can be laborious and time-consuming[10,11], and this issue is further exacerbated by the limited expansion capacity of MSCs in culture systems[12,13]. Therefore, upscaling exosome production is crucial to enable their broader therapeutic application.

To address the aforementioned challenges, this study established a potential upscaling protocol for the production of exosomes derived from canine adipose-derived mesenchymal stem cells (cAD-MSCs). This development combined microcarrier-based 3D culture system with TFF isolation method along with the establishment of in-house exosome-collecting medium. Furthermore, the wound-healing potential of cAD-MSCs-derived exosomes on fibroblast in vitro was explored. This study found increased production yield of cAD-MSCs-derived exosomes produced using the established protocol. In addition, cAD-MSCs-derived exosomes were evident to enhance the migration, proliferation, and expression of genes related to early wound healing, which collectively indicates promising wound treatment potential. This establishment is expected to be a robust strategy to produce cAD-MSCs-derived exosomes that are not only beneficial to enhance wound healing but also practical to be applied for veterinary clinical applications.

Results

Isolated cAD-MSCs demonstrate MSC characteristics

The isolated cAD-MSCs displayed the morphological appearance as the anchorage-dependent cells with fibroblastic-like morphology during the maintenance in a conventional 2D culture system (Fig. 1A-B). The mRNA expression of stemness markers (*Oct4* and *Rex1*) and proliferative marker (*Ki67*) were confirmed by RT-qPCR (Fig. 1C). Flow cytometry analysis indicated the expression of MSC-related surface markers (CD90, CD44, and CD29) and lacking in CD73 expression. Additionally, the absence of the hematopoietic cell surface marker, CD45, was noted (Fig. 1D).

In vitro multilineage differentiation results indicated the osteogenic differentiation capacity, as evidenced by mineralization of the extracellular matrix (ECM) observed through Alizarin red staining, in addition to upregulation of *Osx*, a gene marker associated with osteogenesis (Fig. 1E). Simultaneously, Chondrogenic differentiation potential was demonstrated by the accumulation of glycosaminoglycans stained with Alcian blue dye, although up-regulation of chondrogenic markers (*Sox9* and *Col2a1*) was not observed. This may be due to the early stage chondrogenic differentiation of the cells (Fig. 1F). Adipogenic differentiation potential was confirmed by the detection of intracellular lipid droplets visualized using Oil Red O staining accompanied with upregulations of adipogenic-related gene markers (*Leptin* and *LPL*) (Fig. 1G).

These collective findings indicate that the isolated cAD-MSCs exhibit the MSC characteristics and multilineage differentiation potential.

An in-house exosome-collecting solution, VSCBIC-3, sustains cAD-MSCs viability during the exosome-collecting period

To enhance the efficiency of the exosome collection platform, a series of exosome-collecting solutions were established and validated. The infographic of the study process is summarized in Fig. 2A. In this study, four potential exosome-collecting solutions were validated including the serum-free DMEM (SF-DMEM), the DMEM supplemented with exosome-depleted FBS (dEx-DMEM), the in-house exome-collecting solution (VSCBIC-3), and the in-house exome-collecting solution supplemented with exosome-depleted FBS (dEx-VSCBIC-3). A routinely used growth medium, DMEM supplemented with 10% FBS, was used as a control.

To preliminarily evaluate the efficiency of the exosome-collecting solutions, the morphological appearance of the exosome-producing cells, the canine adipose-derived mesenchymal stem cells (cAD-MSCs), maintained under each exosome-collecting solution was observed along with the cell viability as analyzed by live/dead assay and cell population analysis as assessed by resazurin assay.

For cell morphology, the results illustrated that the VSCBIC-3 and dEx-VSCBIC-3 could maintain cell morphology and attachment till day 3 of the maintenance. However, the dEx-DMEM and SF-DMEM could not

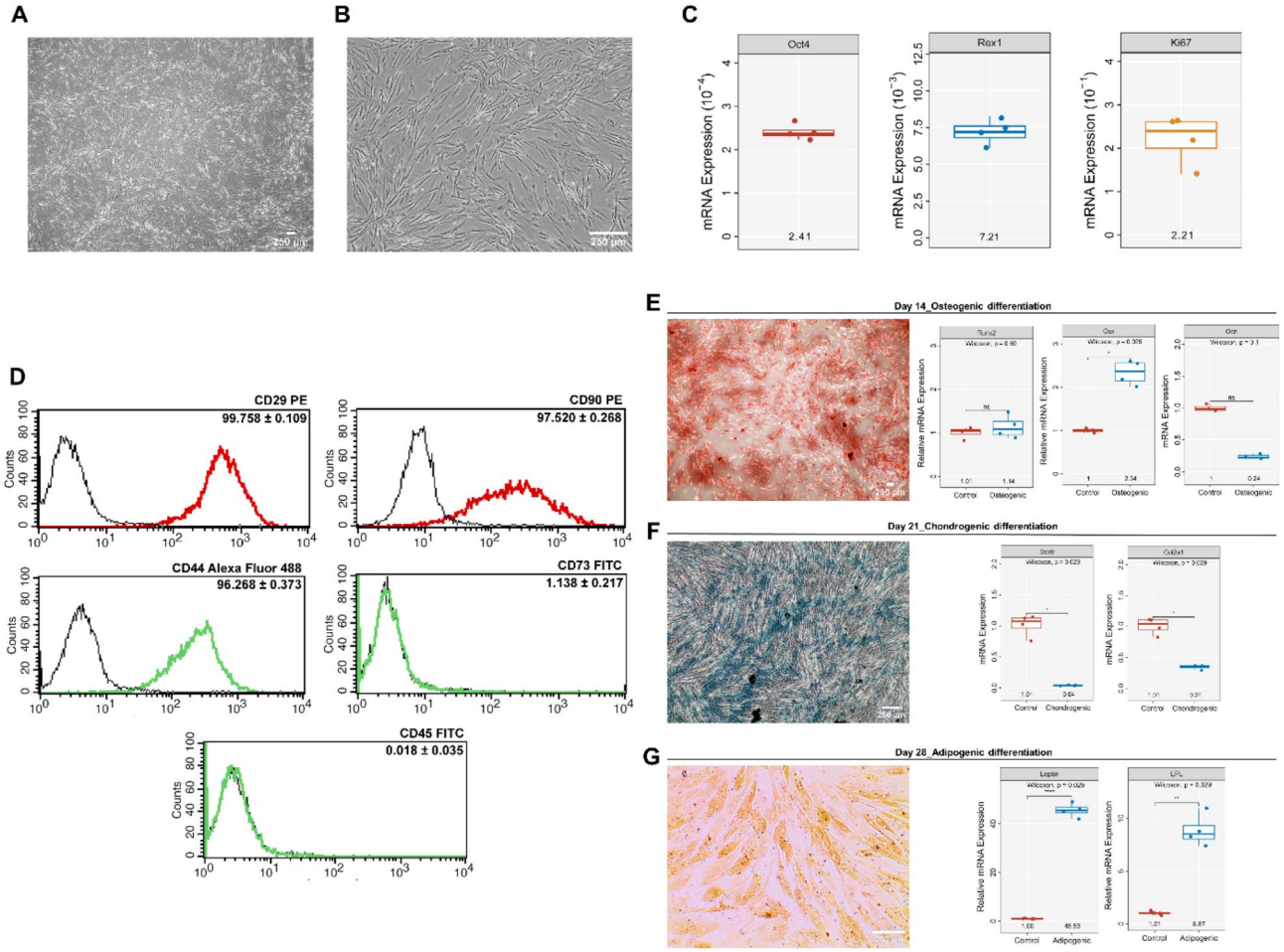

Fig. 1. Characterization of cAD-MSCs. (**A**, **B**) Morphology representation of isolated cAD-MSCs was observed using phase-contrast microscopy at 40X and 200X magnifications. (**C**) Stemness markers (*Oct4 and Rex1*) and proliferative marker (*Ki67*) mRNA expression were assessed via RT-qPCR and normalized to a reference gene (*Gapdh*). (**D**) Expression of MSC and hematopoietic-related surface markers was analyzed using Flow cytometry. (**E**) Osteogenic differentiation potency was identified by Alizarin red staining and analysis of gene expression for osteogenic-related markers. (**F**) Chondrogenic differential potency was determined using Alcian blue staining and chondrogenic-related gene expression analysis. (**G**) Adipogenic differential potency was evaluated through Oil Red O staining and the mRNA expression of adipogenic-related markers. mRNA expression of multilineage differentiation markers was normalized to the reference gene and the undifferentiated group served as control. The mean and *p*-value are depicted, with asterisks denoting the significance levels ($^{*}p < 0.05$, $^{**}p < 0.01$, $^{***}p < 0.001$).

exhibit this effect, and the cells started losing their morphology and attachment since day 2 of the maintenance. It should be noted that some populations of cAD-MSCs maintained by SF-DMEM showed prominent intracellular vacuolization after day 3 under maintenance (Fig. 2B).

Further qualitative analysis on cell viability by live/dead assay revealed that the detection of dead cells was clearly found since day 2 for the cells maintained by SF-DMEM and dEx-DMEM. However, the VSCBIC-3 and dEx-VSCBIC-3 could maintain the viability of the majority of the population until day 3 (Fig. 2C). To assess the beneficial effects of exosome-collecting solutions on cell population, resazurin analysis was performed. A consistent trend was observed in which the VSCBIC-3 yielded the highest number of cell populations until day 3 of the maintenance, while other solutions lacked these effects since day 2, especially dEx-DMEM and SF-DMEM (Fig. 2D).

The findings suggest that an in-house exosome-collecting solution, VSCBIC-3, sustains cAD-MSCs morphology, viability, and population number for at least 3 days which was optimum for the application during the exosome-collecting period.

Potential upscaling protocol enhances cAD-MSC-derived exosome production in both quality and quantity aspects

To enhance the exosome production from cAD-MSCs, three exosome production protocols were established and assessed: (i) 2D-based exosome production platform using SF-DMEM as exosome-collecting medium

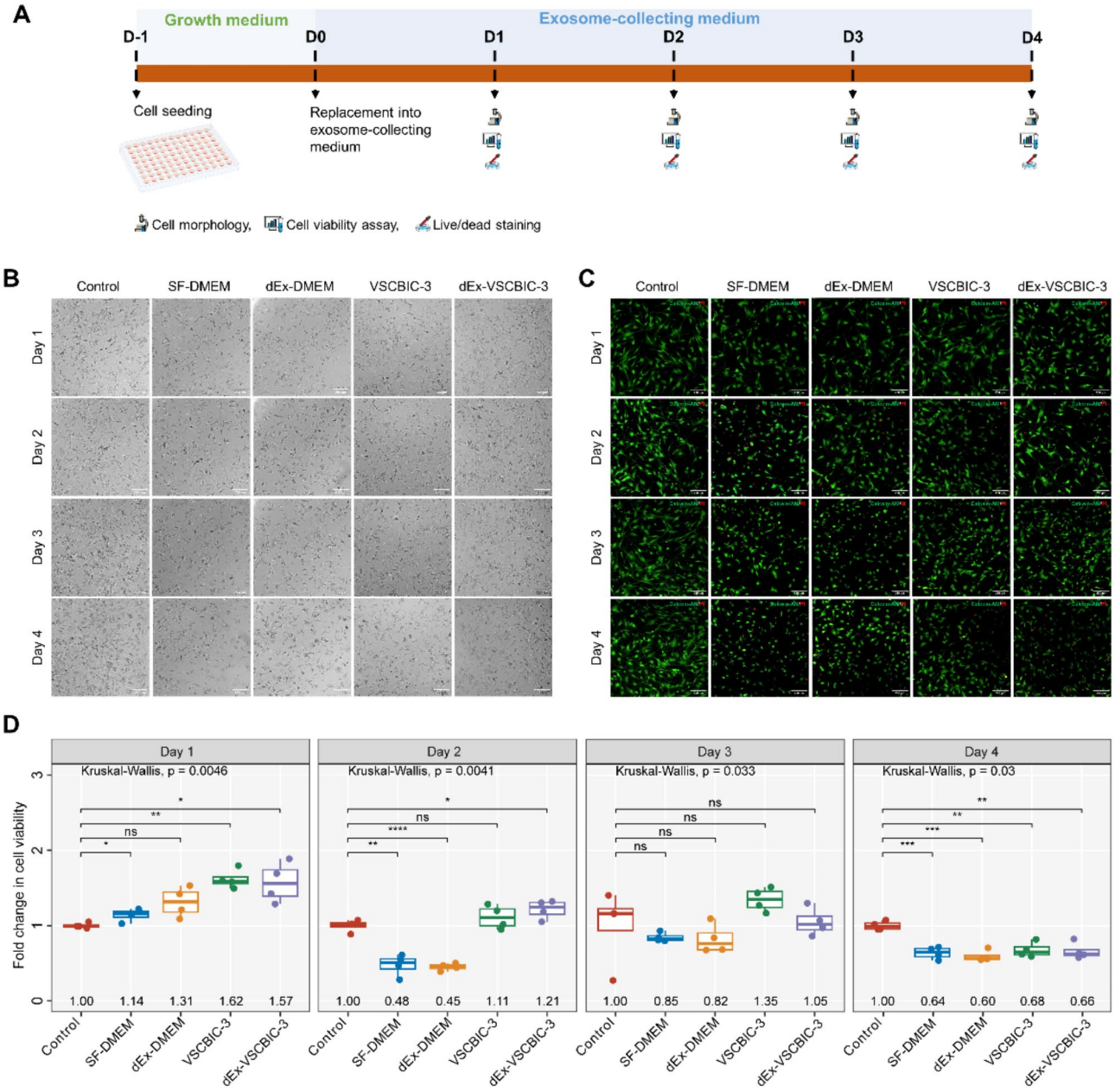

Fig. 2. Establishment of culture medium potential for cAD-MSc exosome collection. (**A**) Schematic of experimental design. (**B**) Morphological representation of cAD-MSCs cultured with various exosome-collecting media investigated at days 1, 2, 3, and 4 of incubation. (**C**) Live/dead staining of cAD-MSCs upon the culture within various exosome-collecting media. Live cells were labeled with green fluorescence using calcein-AM, while dead cells were marked with red fluorescence using propidium iodide. (**D**) The viability of cAD-MSCs cultured in different exosome-collecting media was evaluated using the resazurin assay on days 1, 2, 3, and 4. The results are presented as fold change normalized to the control group for each day of incubation. The mean and *p*-value are denoted ($n = 4$), with asterisks presenting the significance levels compared to the control (*$p < 0.05$, **$p < 0.01$, ***$p < 0.001$). The scale bar indicates 250 µm.

(SF-DMEM-2D), (ii) 2D-based exosome production platform using VSCBIC-3 as exosome-collecting solution (VSCBIC-3-2D), and (iii) 3D-based exosome production platform using VSCBIC-3 as exosome-collecting solution (VSCBIC-3-3D), the schematic workflow of this study is depicted in Fig. 3A, B.

Morphology assessment at the beginning of the conditioning period showed typical fibroblast-like morphology and adherence of cAD-MSCs maintained in 2D-culture system. Meanwhile, in the 3D platform, cells adhered and spread on the microcarrier surface after 24 h of seeding protocol. This indicates a successful cAD-MSC culture in the microcarrier-based 3D system. After undergoing a conditioning period for 48 h, cells began losing morphology and attachment, which was particularly evident in the SF-DMEM-2D group. Similarly,

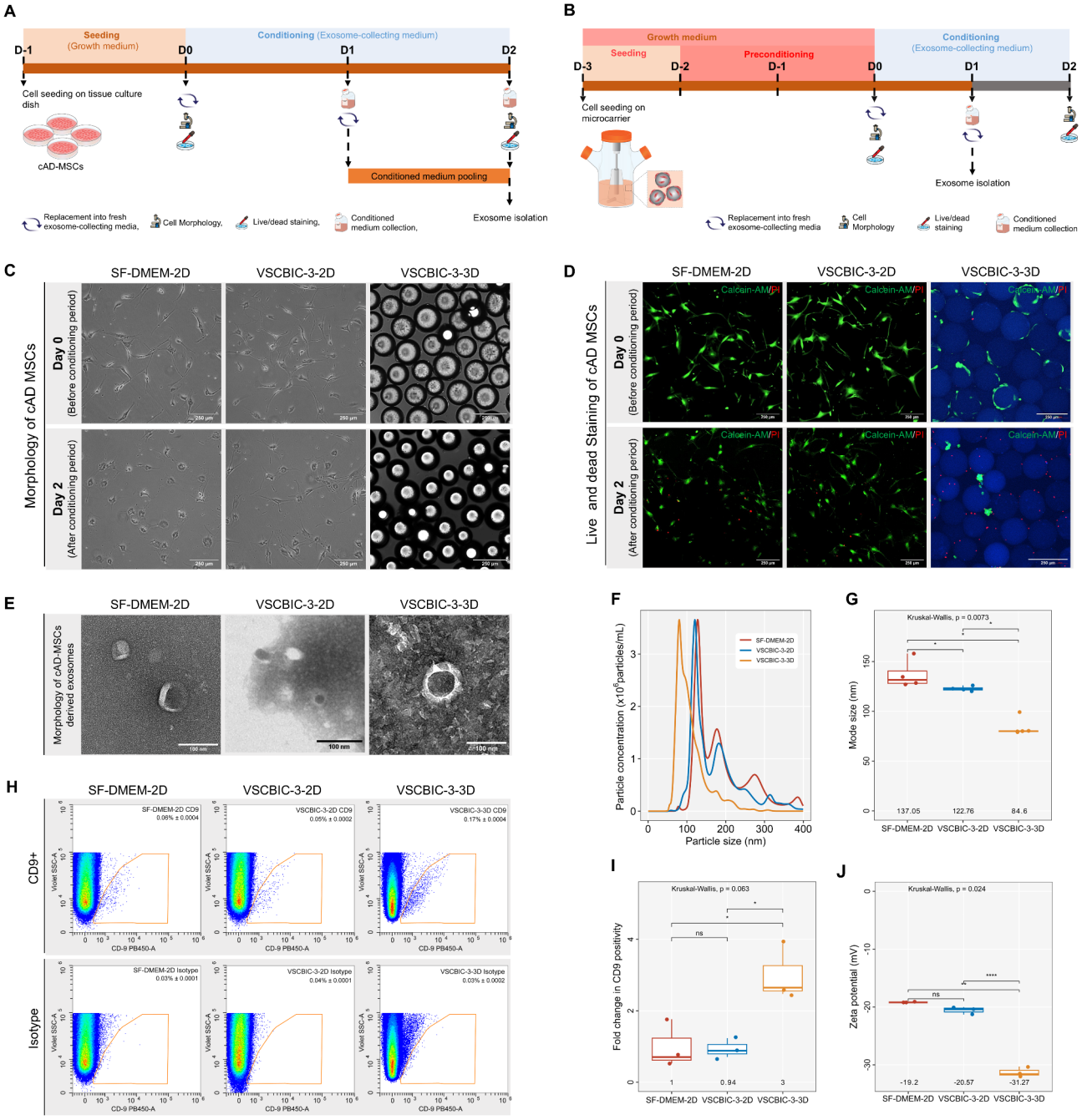

Fig. 3. The impact of exosome production protocols on both cAD-MSCs characteristics and cAD-MSC-derived exosome qualitative specifications. Schematic illustration of (**A**) 2D-based exosome production protocol and (**B**) 3D-based exosome production protocol. (**C**) Morphology representation of cAD-MSCs undergoing exosome production was obtained at the beginning (day 0) and the end (day 2) of the conditioning period. (**D**) Live/dead staining of cAD-MSCs was conducted at the beginning and final days of the conditioning period during exosome production. Live cells were labeled with calcein-AM dye, emitting green fluorescence, while dead cells were stained with propidium iodide dye, emitting red fluorescence. The scale bar indicates 250 µm. (**E**) The morphology of cAD-MSC-derived exosomes isolated from different production protocols was visualized using TEM. The scale bar marked 100 nm. (**F**) Particle size and distribution and (**G**) mode size of cAD-MSC-derived exosomes produced from either 2D platforms or 3D platform were analyzed using NTA. The value indicating mean was plotted ($n = 4$). (**H**) Pseudo-contour diagram generated from Nano-scale flow cytometry analysis illustrating gates of CD9+ exosome produced from different protocols. The mean ± SD are plotted ($n = 3$). (**I**) CD9 positivity of exosome was generated from nano-scale flow cytometry findings. The results are presented as fold change normalized to the exosome from SF-DMEM-2D as control. The mean and p-value are denoted ($n = 4$). (**J**) Zeta potential value of cAD-MSC-derived exosome obtained from various production protocols. The mean and p-value are plotted ($n = 3$). The asterisks illustrate the significance levels (*$p < 0.05$, **$p < 0.01$, ***$p < 0.001$).

cells cultured in the VSCBIC-3-3D platform also displayed a loss of cell morphology, along with detachment and cell aggregation at the surface of the bead (Fig. 3C).

Live/dead analysis performed upon the exosome collection revealed the presence of dead cells from cultures maintained in the 2D system. Unexpectedly, significant numbers of dead cells were also noted from cultures in the 3D system after 2 days of maintenance in exosome-collecting medium, while the remaining live cells were stained with calcein-AM aggregating on the surface of microcarriers (Fig. 3D). These findings suggest that replacement into the exosome-collecting medium affected the morphology and viability of cAD-MSCs maintained in both 2D and 3D culture systems.

Subsequently, qualitative characteristics of exosomes obtained from different protocols were analyzed and compared. Transmission Electron Microscopy (TEM) assessment revealed the presence of vesicles with distinct cup-shaped morphology and diameter < 200 nm in samples from all production protocols (Fig. 3E). This observation was supported by NTA results, indicating a consistent monodisperse size distribution among samples from all groups, with the particle mode size falling within the exosome size range of 50–200 nm (Fig. 3F). Remarkably, VSCBIC-3-3D-exosomes exhibited a significantly smaller mode size (84.6 ± 9.75 nm; $p < 0.05$) compared to VSCBIC-3-2D-exosomes (122.76 ± 2.51 nm) and SF-DMEM-2D-exosomes (137.05 ± 14.41 nm) (Fig. 3G).

Nanoscale flow cytometry analysis consistently detected a low presence of CD9+ particles within the exosome size range (Fig. 3H). However, a threefold increase in CD9 positivity was noted in VSCBIC-3-3D-exosome populations compared to other groups, albeit without significant differences observed (Fig. 3I). Zeta potential analysis revealed that VSCBIC-3-3D-exosomes exhibited a significantly more negative surface charge (-31.27 ± 0.9, $p < 0.01$) compared to exosomes obtained from VSCBIC-3-2D (-20.6 ± 0.07) and SF-DMEM-2D at (-19.2 ± 0). Moreover, it is interesting to note that zeta potential analysis consistently showed a negative surface charge in exosome samples from all groups, indicating improved colloidal stability (Fig. 3J). These collective findings indicate the typical exosome characteristics were detected in samples from all production protocols.

In order to evaluate productivity among different protocols, exosome quantitative characteristics were compared as illustrated in Fig. 4A. Exosome yield production was determined by dividing the total particle

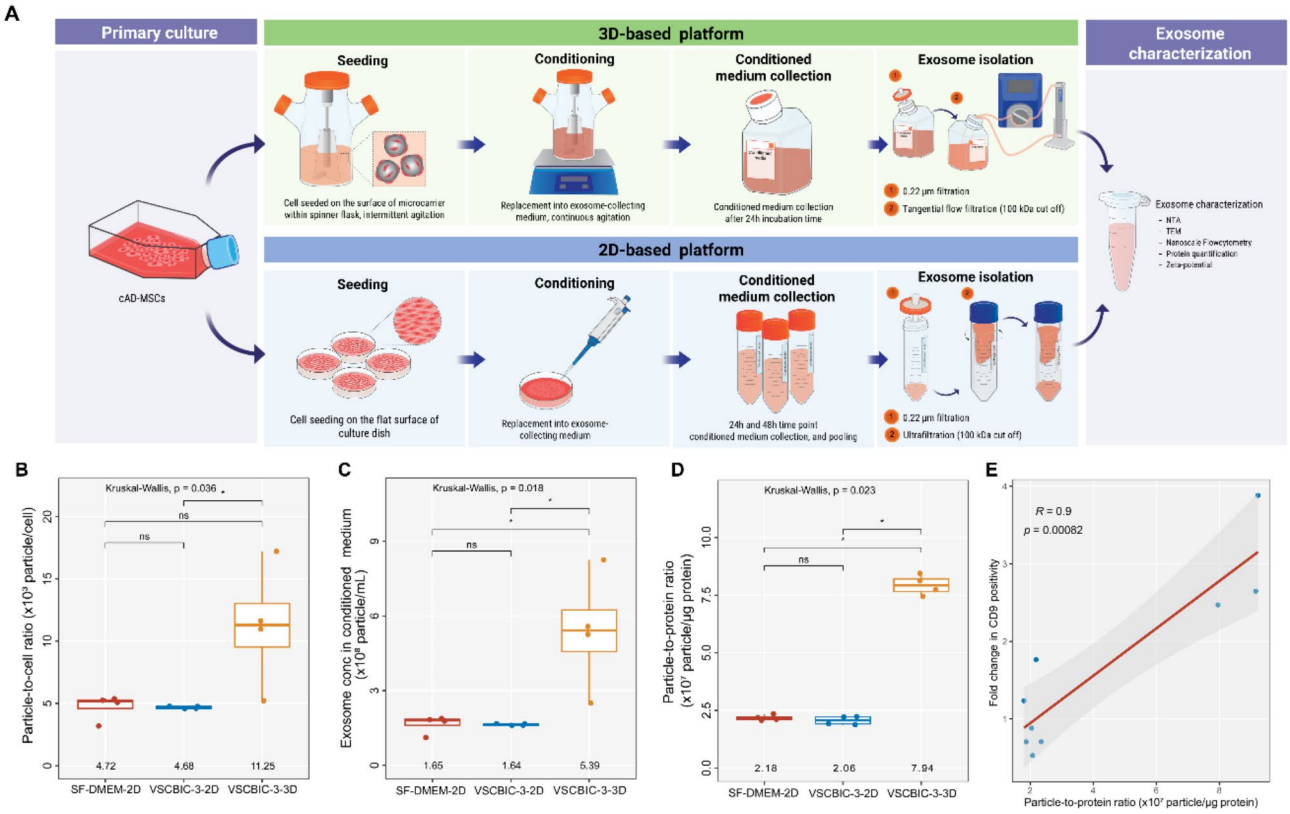

Fig. 4. Quantitative and productivity assessment of cAD-MSC-derived exosome production protocols. (**A**) Schematic workflow of exosome production. (**B**) Production yield comparison, calculated by total particle production analyzed from NTA divided by initial cell seeding number in various production protocols ($n = 4$). (**C**) Comparison of exosome concentration (particle/mL) in conditioned medium of cell cultured using different production protocol ($n = 4$). (**D**) The ratio of particle number to microgram protein obtained from different exosome production protocols. The mean and p-value are noted. (**E**) Pearson's correlation coefficient between the particle-to-protein ratio and CD9 positivity, obtained from exosome characterization across all groups ($n = 9$). R-value and p-value are plotted. The asterisks indicate the significance levels (*$p < 0.05$, **$p < 0.01$, ***$p < 0.001$).

number, calculated from NTA, by the initial cell seeding number. The results indicated comparatively higher production yield by VSCBIC-3-3D protocol, at approximately 2.4-folds ($p < 0.05$), compared to exosome yield from both 2D platform production (Fig. 4B). Interestingly, the VSCBIC-3-3D protocol also produced a higher exosome concentration in the conditioned medium compared to the other 2D production. This further implies that to obtain an equivalent exosome particle amount, the VSCBIC-3-3D protocol required approximately 3.2 times less exosome-collecting medium (Fig. 4C).

Particle-to-protein ratio was calculated by dividing the particle concentration (particle/mL), determined using NTA, by the protein concentration (µg/mL), determined by the protein quantification assay. Particle-to-protein ratio of exosome samples obtained from SF-DMEM-2D and VSCBIC-3-2D was comparatively similar, while a significantly higher ratio was observed by VSCBIC-3-3D-exosome, at approximately 4-fold ($p < 0.05$) (Fig. 4D). Additionally, a significant correlation was exhibited between particle-to-protein ratio and fold change in CD9 positivity ($r = 0.9$, $p = 0.0082$), these two variables are associated to the exosome sample purity. These findings suggest that the quality of isolated exosomes differs between 2D and 3D-based production protocols (Fig. 4E). The aforementioned results suggest similarities in the production profile between SF-DMEM-2D and VSCBIC-3-2D protocols. Meanwhile, VSCBIC-3-3D protocol demonstrated enhanced exosome production quality and quantity. In this regard, VSCBIC-3-3D exosome production is considered suitable as a potential upscaling protocol.

cAD-MSC-derived exosomes produced from potential upscaling protocol show wound treatment potential in vitro

Three-dimensional exosome production provides beneficial effects on wound healing in vitro

In addition to productivity, bioactivity was another essential consideration in developing exosome upscaling production. The bioactivity of exosomes obtained from various production protocols was evaluated by an in vitro migration assay as illustrated in Fig. 5A.

Representative images demonstrated cells migrated across the wound gap over the course of the treatment, while cAD-MSC-exosome-treated cells illustrated enhanced cell migration compared to the control (Fig. 5B-D). To accurately evaluate and compare the efficacy of cAD-MSC-exosome treatment, the closure rate was calculated. The gap area, measured from each experimental frame using NIS-Elements Advanced Research (Nikon), was plotted against incubation time variables using the linear trendline function in Excel. Hence, the slope derived from the equation serves as the gap closure rate, representing the velocity at which cells migrate collectively toward the gap[14].

During the 0–12 h incubation period, a significant increase of closure rates was exhibited by exosome-treated groups compared to the untreated control this beneficial effect was enhanced within the increasing of exosome concentration (Fig. 5E). A similar trend was maintained during the 12–24 h incubation period, hence only VSCBIC-3-3D-exosomes indicating significantly higher closure rates compared to the control (Fig. 5F). The consistent trend observed in the overall closure rate analysis (0–24 h incubation time) further confirmed the enhanced effect of cAD-MSC-derived exosomes on fibroblast migration in vitro (Fig. 5G). Interestingly, the higher concentration of VSCBIC-3-3D-exosomes tends to demonstrate increased fibroblast migration. While both 5×10^7 particle/mL and 10^8 particle/mL demonstrated a comparable effect, the former at 5×10^7 particle/mL was deemed the cost-effective dose of VSCBIC-3-3D-exosomes.

These collective findings indicate the beneficial effect of the potential upscaling protocol, VSCBIC-3-3D protocol, on exosome wound healing activity. Therefore, VSCBIC-3-3D-exosomes were selected to investigate further the phenotypic and genotypic effect of cAD-MSC-exosomes on fibroblasts in vitro.

cAD-MSC-derived exosomes produced from potential upscaling protocol exhibit phenotypic and genotypic wound treatment potential in vitro

To further explore its potential, exosomes produced from VSCBIC-3-3D (VSCBIC-3-3D-exosomes) were subsequently subjected to in vitro proliferation assay as demonstrated by Fig. 6A. One-day proliferation assay evaluated the immediate effect of VSCBIC-3-3D-exosomes on fibroblast proliferation over a day of treatment. Morphological analysis exhibited no noticeable alterations in cell appearance following exosome treatment compared to the control group. Live/dead staining revealed a minimal number of dead cells across all groups, indicating no cytotoxic effects attributed to VSCBIC-3-3D-exosome treatment on fibroblasts (Fig. 6B). The resazurin assay revealed enhanced cell proliferation in all exosome-treated groups, with a 1.3 to 1.7-fold increase compared to the control. Although cell proliferation response to increasing VSCBIC-3-3D-exosome concentration slightly fluctuated, higher concentrations of the VSCBIC-3-3D-exosomes, particularly at 10^7 and 5×10^7 particle/mL, exerted a greater impact on fibroblast proliferation (Fig. 6C).

To assess the beneficial effects of VSCBIC-3-3D-exosome treatment in continuous cell culture, the proliferation assay was conducted sequentially over a 4-day incubation period (Fig. 6D). However, due to the cells' dependency on serum supplementation, the experimental setup was modified by adding 3.5% FBS to the basal medium, which also served as the untreated control group. Loss of cell morphology and detachment was increasingly evident in the untreated control after 2-day incubation, while cells treated with VSCBIC-3-3D-exosomes in various concentrations were able to sustain cell morphology with minimal detachment observed until day 3 of incubation (Fig. 6E). Live/dead staining revealed an increasing number of dead cells after day 2 of incubation, which was particularly noticeable in the control group. On the contrary, exosome-treated groups showed an increasing number of live cells over the course of treatment (Fig. 6F). The Resazurin assay result in Fig. 6G indicates the effect of VSCBIC-3-3D-exosome treatment on cell proliferation. Although no significant difference was observed in the first two days of maintenance that possibly was caused by cellular adaptation, cell proliferation significantly increased by day 3. This impact was observed dose-dependently, albeit the slight fluctuation. This effect continued on day 4, in which the VSCBIC-3-3D exosomes treated groups predominantly

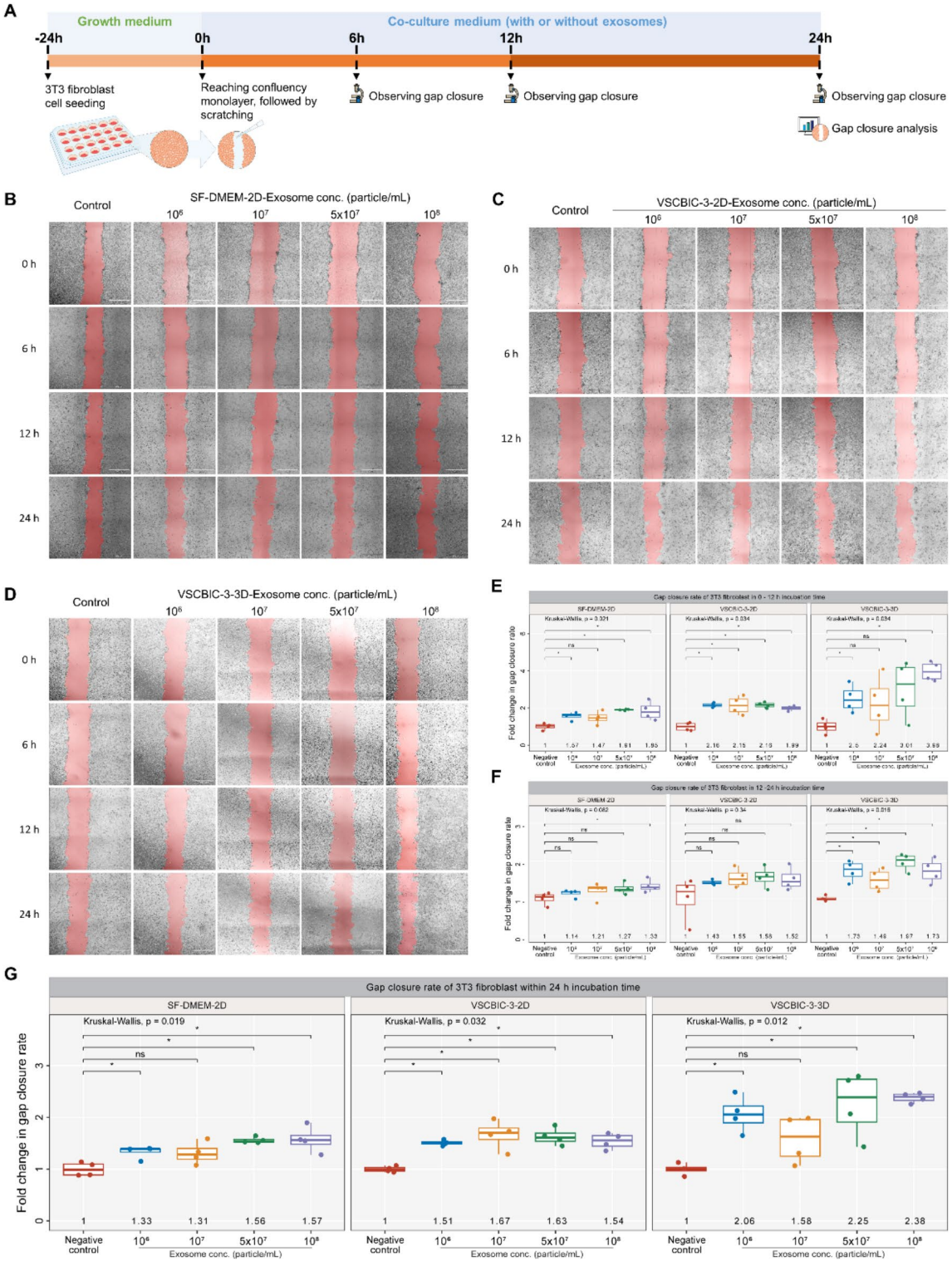

Fig. 5. cAD–MSC–derived exosomes produced by potential upscaling protocol enhanced the migration of fibroblast in vitro. (**A**) Illustrative diagram depicting in vitro migration assay. (**B**–**D**) images representing gap closure assessment of cells without or with exosome treatment from various production protocols. The red region marked the wound gap area, analyzed using NIS-elements software. (**E**–**G**) Closure rate analysis illustrates the response of cells to exosome treatment during (**E**) 0–12 h incubation, (**F**) 12–24 h incubation, and (**G**) overall 24 h observation. The data ($n = 4$) are presented as fold change, normalized with the untreated control group in each experimental setup. The mean and p-value are noted. The asterisks suggest the significance levels ($^{*}p < 0.05$, $^{**}p < 0.01$, $^{***}p < 0.001$).

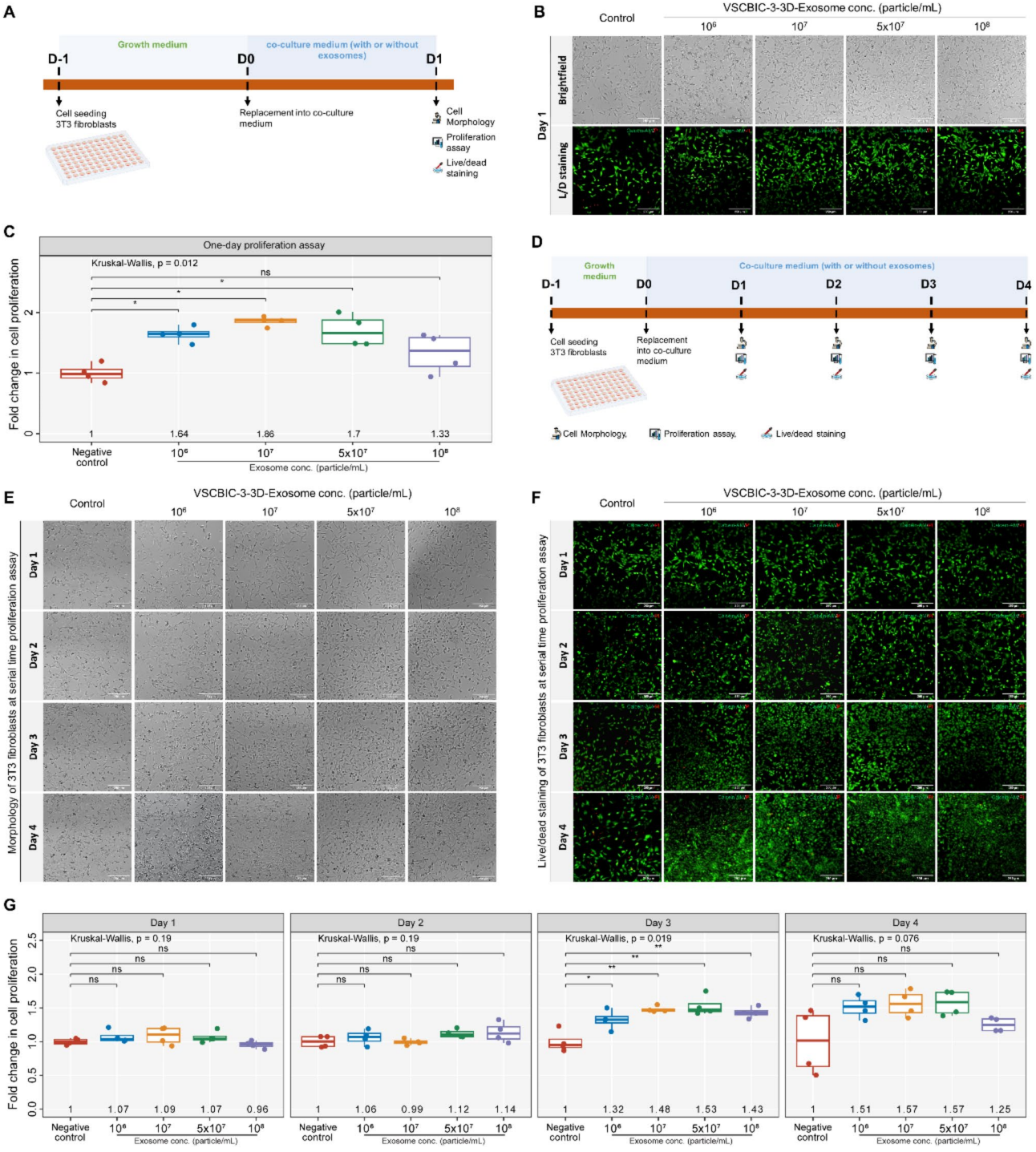

Fig. 6. Improved Fibroblast Proliferation in vitro induced by cAD-MSC-derived exosomes at various concentrations. (**A**) schematic illustration of the single time point proliferation assay. (**B**) Representative images depicting the morphology and live/dead staining of fibroblasts after 24 h of treatment with different concentrations of exosomes. (**C**) Cell proliferation was assessed using a resazurin assay to evaluate the impact of exosome treatment at varying concentrations during a 24-hour incubation period. The values are presented as fold change, normalized with the untreated control. (**D**) Schematic workflow of serial time point proliferation assay. (**E**) Representative brightfield images depicting the morphology of fibroblasts at days 1, 2, 3, and 4 of incubation. (**F**) Live/dead staining of fibroblast co-cultured within varying concentrations of cAD-MSC-derived exosomes over 4 days incubation. (**G**) Cell proliferation analysis compared the effect of exosome treatment at various concentrations over 4-day incubation period. The values are illustrated as fold change, normalized with the basal medium control in each day. The mean and *p*-value are plotted, while asterisks indicating the significance levels compared to the control (*$p < 0.05$, **$p < 0.01$, ***$p < 0.001$). The scale bar indicates 250 µm.

showed higher cell proliferation compared to the control, despite not being statistically significant. These results collectively implied that VSCBIC-3-3D-exosome treatment potentially promotes fibroblast survival and proliferation in vitro.

To further evaluate the beneficial effect of VSCBIC-3-3D-exosomes as wound treatment, the mRNA expression of genes related to different stages of wound healing and glucose utilization was analyzed at 24 h post-treatment. It is evident that VSCBIC-3-3D-exosomes led to increased expression of *Tgf-β1*, a wound healing-related marker involved in the early proliferation stage, despite the variation in the expression level attributed to exosome concentration. In contrast, downregulation of genes encoding for *Tgf-β3* and *Col3a1* was observed, however, this expression was associated with the later stage of the remodelling phase. Treatment of the VSCBIC-3-3D-exosomes also induced the upregulation of *TNF-α*, a potent inflammatory cytokine known to be involved in the inflammation stage and early proliferation stage. Subsequently, the upregulation of glucose utilization-related marker, *Glut1*, was also found in the dose-dependent manner (Fig. 7A-B). Interestingly, Pearson's correlation analysis revealed significant associations among gene expressions. The expression of *Tgf-β3* exhibited a significant positive correlation with *Col3a1* ($r = 0.931$, $p < 0.001$), while it negatively correlated with *TNF-α* ($r = -0.721$, $p < 0.001$) and *Glut1* ($r = -0.731$, $p < 0.001$). The mRNA expression of *Col3a1* negatively correlated with *TNF-α* ($r = -0.691$, $p < 0.01$) and *Glut1* ($r = -0.532$, $p < 0.05$). A significant positive correlation was also found between *TNF-α* and *Glut1* expression ($r = 0.625$, $p < 0.01$) as depicted in Fig. 7C. Collectively, the wound healing potential of VSCBIC-3-3D-exosomes was evidenced by the improved fibroblast migration, proliferation and mRNA expression of wound healing related and glucose utilization markers in vitro.

Discussion

Emerging studies have investigated the therapeutic potential of MSC-derived exosomes for various clinical applications including wound healing. However, to date, its translation to clinical practice faces challenges due to the lack of an efficient production protocol to obtain a clinically relevant exosome quantity. Hence, this study aimed to establish a potential upscaling protocol for exosome production from cAD-MSCs and explore its wound treatment potential in vitro.

The isolated cAD-MSCs possessed the typical characteristics of MSCs as defined by the International Society for Cellular Therapy (ISCT)[15] which includes the plastic adherent property, expression of MSC-related surface markers, and multi-lineage differentiation potency. In addition, we identified the mRNA expression of pluripotent (*Oct4* and *Rex1*) and proliferative (*Ki67*) markers, which implies the cells' stemness and proliferative ability. Correlated to ISCT requirements the high percentage of CD44, CD90, and CD29 positive cells was observed, although in the absence of CD73 expression. Low or absent expression of CD73 has been reported previously in MSCs derived from canine[16–19] and feline[20] sources. This suggests the difference in CD73 expression between animal-derived MSCs and those from human sources, as referenced in ISCT guidelines. Furthermore, the isolated cAD-MSCs demonstrated differentiation potential towards osteogenic, adipogenic, and chondrogenic lineages, confirmed through either phenotypic or genotypic assessments[21,22].

This study demonstrates that VSCBIC-3 in-house exosome-collecting solution effectively preserved the viability of cAD-MSCs compared to SF-DMEM and dEx-DMEM. Notably, the VSCBIC-3 solution is a serum-free-based medium supplemented with chemically defined components. These suggest that the absence of serum and supplementation, demonstrated by SF-DMEM and dEx-DMEM, during exosome collection may be attributed to the decline in cell population number and increased cell detachment observed in this study. The removal of serum from the culture medium is critical upon exosome collection. This prevents the potential co-isolation of exogenous extracellular vesicles (EVs) and soluble particles originating from serum. Such contaminants could interfere with the authentic potential of MSC-derived exosomes and inadvertently induce side effects[23,24]. While the serum depletion method has been explored, it may be impractical for upscaling production and lead to batch-to-batch variation[25].

Correlated to the current study, prior research has demonstrated the impact of serum deprivation during exosome collection on cell phenotype and viability. These are possibly due to the reduced cellular metabolic activity and elevated oxidative stress levels that eventually affect cell viability and phenotype[25]. Moreover, a study reported the co-occurrence of extensive apoptosis within the cell culture along with abundant detection of calnexin, an endoplasmic reticulum (ER) marker, within the exosome sample[24]. This suggests a potential contamination of apoptotic bodies. Hence, maintaining cell viability becomes an essential consideration in establishing exosome-collecting medium and ensuring the quality of exosome production. VSCBIC-3 in-house exosome-collecting solution was eventually selected in this research to establish a potential upscaling protocol for exosome production.

Microcarrier-based 3D culture systems are gaining traction due to their ability to provide a larger surface area for adherent cell culture in bioreactors, facilitating efficient upscale production[13,26]. The current study demonstrated successful maintenance of cAD-MSC in 3D culture conditions. Additionally, phenotypic changes were noted during cell conditioning in both 2D and 3D culture systems, possibly influenced by cell maintenance in the exosome-collecting medium. Previous study indicates that using a xeno-free medium for MSCs in 3D culture resulted in low cell attachment. This outcome was associated with the inactivation of FAK signaling pathways, likely leading to the induction of anoikis in the cells[27]. The formation of cell aggregation in microcarrier cultures often occurs due to reduced cell-surface adhesion, leading to increased susceptibility to detachment influenced by hydrodynamic forces[28,29]. However, this phenomenon is known to be reversible[28,30], as evidenced by our findings of improved cell viability and attachment upon reverting to a growth medium containing 10% FBS for 2 days (Supplementary Figure S1). This may suggest the potential reproducibility of exosome production from a consistent cell source.

This study aimed to establish a potential upscaling protocol for efficient and practical exosome production. To achieve this, we evaluate platforms used both in the upstream and downstream production: comparing 2D and

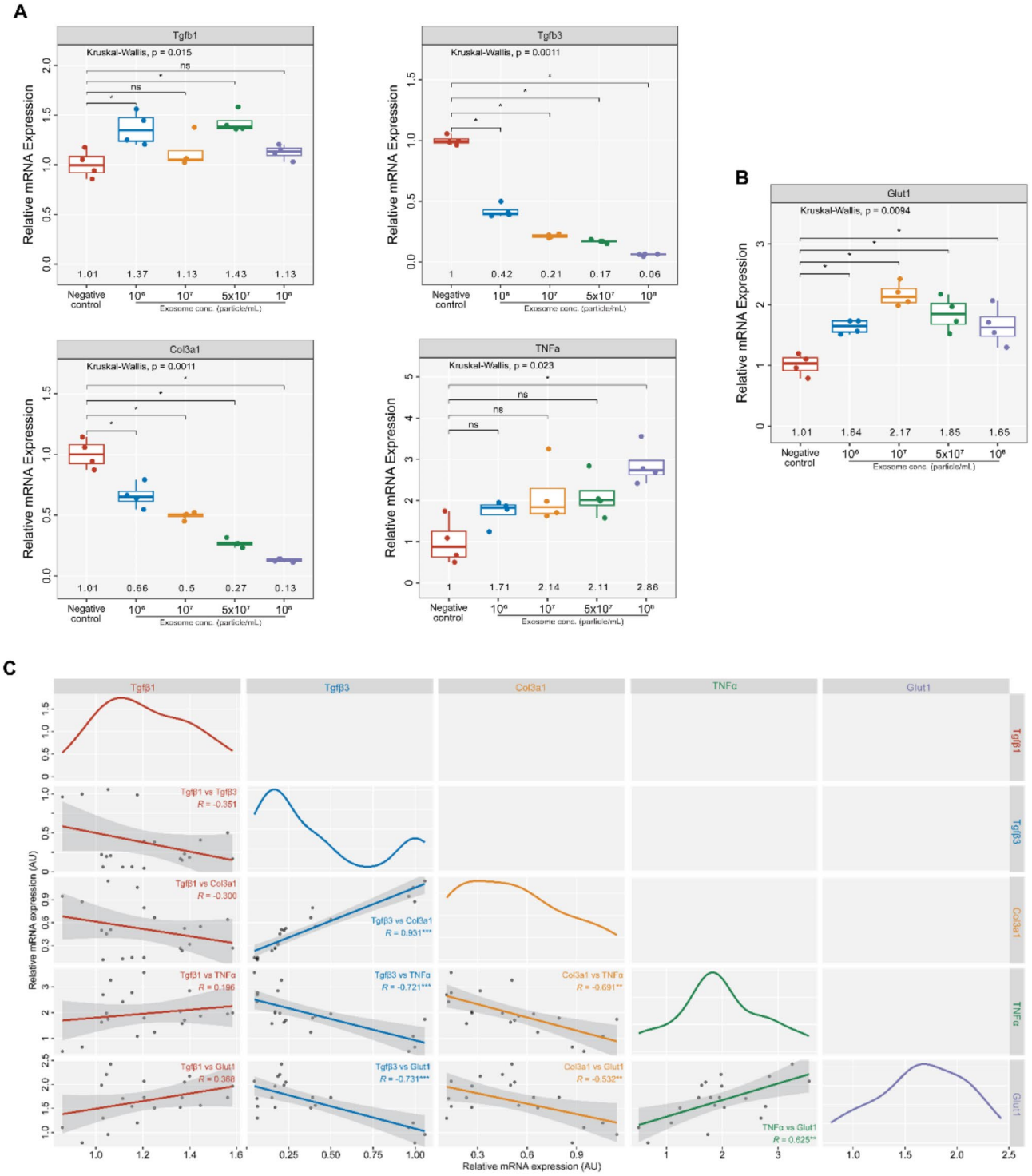

Fig. 7. The impact of cAD-MSC-derived exosome treatment on fibroblast gene expression in vitro. mRNA expression of (**A**) wound healing-related markers, including *Tgfβ1*, *Tgfβ3*, *Col3a1*, *TNFα*, and (**B**) glucose utilization marker *Glut1*, was observed using qRT-PCR after 24 h of treatment. The mean and *p*-value are denoted. (**C**) Pearson's correlation analysis across different gene marker expressions related to the effect of cAD-MSC-derived exosome treatment on fibroblast in vitro. The asterisks illustrate the significant levels compared to the control (*$p < 0.05$, **$p < 0.01$, ***$p < 0.001$).

3D culture systems for upstream production and assessing Tangential Flow Filtration (TFF) and Ultrafiltration (UF) for downstream processing. On the other hand, TFF is a notable high-throughput filtration, making it an efficient tool for isolating exosomes from larger volumes of conditioned media[31]. Meanwhile, producing a large batch of conditioned media in a 2D culture system may demand the amplification of monolayer culture

involving the usage of abundant culture flasks, which eventually becomes labor- and cost-intensive[26,32]. In the long run, this approach may lead to scaling out production which is not aligned with our study's scalability objectives.

In addition, our design controlled key variables in the isolation process to minimize the potential impact of different isolation methods on exosome characteristics. Specifically, we maintained the consistency of the molecular weight cut-off of the membrane and concentration factor of exosome samples derived from different tested protocols. These measures ensured that any observed differences in exosome yield and purity were genuinely due to established protocol effects rather than variability in isolation conditions, thereby reinforcing the validity of our results.

Our findings confirmed the exosome production across all groups, as evidenced by the presence of typical exosome characteristics in the samples. The quantitative profiles of exosome production further revealed similar trends for SF-DMEM-2D and VSCBIC-3-2D protocols, suggesting that exosome productivity was not influenced by the choice of conditioned medium, whether SF-DMEM or VSCBIC-3. In contrast, the VSCBIC-3-3D protocol demonstrated enhanced productivity, marked by 2.4 times higher exosome yield and 3.2-fold increased exosome concentration in the conditioned medium compared to VSCBIC-3-2D protocol. This may correspond to the cumulative effect of the microcarrier-based 3D culture system and the TFF isolation method utilized in the VSCBIC-3-3D protocol.

In comparison to conventional 2D culture, microcarrier-based 3D culture allows the increasing ratio of surface area to volume of medium[33], thus decreasing the demand for collecting medium for efficient exosome production[10,34]. According to the previous study, increasing productivity correlates to enhanced exosome secretion by cells during 3D culture condition. Dynamic culture parameters, including agitation and shear stress, reportedly promote the exosome secretion from MSCs[35–37]. Enhanced expression of EV biogenesis markers, namely Rab27a and Rab27b, was also reported by cells cultured in the 3D platform compared to the conventional 2D platform[35,38]. Moreover, the efficiency of the isolation method is also known to impact productivity. For potential upscaling protocol, TFF was selected for exosome isolation from larger volumes of conditioned medium. Comparative studies have reported higher production yield and scalability owned by the TFF exosome isolation method compared to conventional methods such as differential ultracentrifugation[12,39].

While the number of cells can indeed affect the overall yield of exosomes, our study specifically analyzed exosome yield using the particle-to-cell ratio. By normalizing exosome particles to the number of seeding cells in each protocol, this indicator reflects exosome production per cell, providing a consistent basis for comparison across all protocols.

In addition, this study also considered various cultural parameters known to influence exosome production as highlighted in previous research. In particular, cell density has been proven to significantly affect the yield of exosomes, with lower densities generally resulting in higher production[40,41]. Based on this foundation, our study maintained a constant cell density involved in both 2D and 3D culture conditions, allowing reliable comparison of the tested platform.

This study compared exosome production quality by analyzing parameters including particle-to-protein ratio, CD9 positivity, and zeta potential. The results showed a similar trend from these parameters observed, in which SF-DMEM-2D-exosomes and VSCBIC-3-2D-exosomes indicated comparatively similar values, while collectively VSCBIC-3-3D showed improved exosome quality. This result implies that differences in exosome quality are independent of the collection medium, between SF-DMEM and VSCBIC-3, but rather depend on cell culture conditions and isolation techniques. A significant correlation was detected between the particle-to-protein ratio and CD9 positivity, both serving as indicators of exosome purity[42,43]. Our results reveal a higher particle-to-protein ratio and CD9 positivity attributed to VSCBIC-3-3D-exosomes compared to exosomes obtained from both SF-DMEM-2D and VSCBIC-3-2D. This may be associated with lower protein contamination in the sample from the VSCBIC-3-3D-exosomes.

Referring to the MISEV2023 guidelines, we assessed the quality of exosome samples by analyzing indicators, such as the expression of markers for specific exosome populations. Additionally, metrics including the particle-to-protein ratio are recommended to approximate exosome abundance. Although MISEV2023 does not recognize universally accepted markers for defining exosomes, CD9 remains a putative marker of tetraspanins-enriched exosome populations[44,45]. Related to our findings, despite its low overall expression, CD9 positivity has consistently been used to examine exosome sample purity across platforms[41,46]. Moreover, it is important to note that not all exosome populations display this tetraspanin. Notably, a study showed that CD9 knockout in mice reduced exosome levels but did not diminish production[47], which highlights the various exosome biogenesis pathways, many of which are not reliant on tetraspanins. However, our study encountered some challenges since EV studies have been primarily human-oriented. The unavailability of commercially produced anti-dog antibodies tailored for detecting exosome surface antigens limited our examination. Taking this into account, we aim to expand this approach in future research to further enhance our understanding.

Fibroblasts play a significant role in wound healing, their migration and proliferation in wound sites are significant in stimulating collagen synthesis and tissue remodeling[5,48,49]. Our study assessed the bioactivity of exosomes from different production protocols using an in vitro migration assay. The findings demonstrated that cAD-MSC-exosomes produced from all given protocols promote the migration effect of fibroblast compared to untreated control. Furthermore, similar trends were observed in exosome-induced fibroblast migration for both 2D culture-based protocols, either using VSCBIC-3 or SF-DMEM as the collection media. On the contrary, the VSCBIC-3-3D exosomes appeared to enhance fibroblast migration.

In addition, VSCBIC-3-3D-exosomes were evident to improve fibroblast proliferation and induce expression of genes related to glucose utilization and the early stage of wound healing. Studies have reported the role of *Tgf-β* isoforms during different stages of wound healing[50,51], correlated to our findings, the upregulation of *Tgf-β1* and downregulation of *Tgf-β3* have been associated with the early stage of proliferation, in which *Tgf-β1* plays an

essential role as chemoattractant for fibroblast and collagen deposition stimulator, while expression of *Tgf-β3* during early wound healing may be associated to inhibition of granulation tissue formation. Conversely, *Tgf-β3* and *Col3a1* expression are correlatedly important during the later stage of the remodeling phase, facilitating fine-tuning of collagen deposition and exerting an anti-fibrotic effect which eventually promotes scarless wound healing[51–53]. Similarly, the upregulation of *TNF-α* during the early stage of the proliferation phase is essential for initiating chemotaxis and proliferation of fibroblast, although prolonged *TNF-α* expression may associated with chronic wound. Several studies have reported enhanced fibroblast activity upon the supplementation of *TNF-α*[54–56]. The aforementioned evidence possibly contributes to the effects of cAD-MSC-exosome treatment on fibroblasts via autocrine or paracrine pathways. In addition, the cAD-MSC-exosome effect on enhanced fibroblast activity may correlated to cellular glucose uptake and metabolism, which was evidenced by the upregulation of *Glut1*[57]. Given the wound healing effect of cAD-MSC-exosomes on fibroblast, the extended effect of exosome treatment on various cell types and phases involved in wound healing remains to be discovered.

The enhanced purity and bioactivity observed in exosomes produced using VSCBIC-3-3D production likely reflects the efficiency of both downstream and upstream processing. In upstream production, the 3D culture system has been demonstrated to promote exosome secretion, resulting in higher exosome yield. This increase may correspond to a higher particle count relative to the particle content, as suggested by our Pearson's correlation analysis, revealing a significant positive correlation between particle concentration and the particle-to-protein ratio ($r = +0.849$, $p < 0.001$, Supplementary Fig. S2). Meanwhile, comparative studies have found no significant difference in the particle-to-protein ratio between exosomes derived from 2D monolayer and 3D microcarrier-based culture[33,42]. This may suggest that while the 3D culture system allows enhanced exosome purity, this impact may also be influenced by another contributing factor in the VSCBIC-3-3D protocol, such as isolation methods.

The implementation of tangential flow filtration (TFF) in downstream processing may also be responsible for the enhanced exosome purity observed in the VSCBIC-3-3D protocol, in comparison to conventional ultrafiltration (UF) used in 2D culture protocols. Unlike conventional dead-end UF, which forces the sample perpendicularly through the membrane and retains dead-end volume leading to the accumulation of contaminant proteins, TFF allows continuous tangential flow of sample across the membrane surface. This mechanism facilitates progressive dilution and minimizes membrane fouling, thus ensuring more efficient contaminant removal[39,58]. In addition, TFF also reduces the shear stress damage on exosomes, preserving their structural integrity and retention of their bioactive cargoes, such as protein and microRNA[12].

In terms of the effect on exosome bioactivity, the 3D culture has been shown to modulate MSCs in secreting exosomes enriched in therapeutic factors. This leads to improved effects on anti-inflammatory responses[59], immune modulation[38,60], neuroprotective properties[61], fibroblast activity[59,62], and wound-healing properties[62]. This enhanced bioactivity is attributed to distinct molecular alterations, including the enrichment of signaling proteins (e.g. collagen type I and FGF) and microRNAs (e.g. miR-20a, miR21, and miR-182)[36], which have been reported to be involved in cellular signaling pathways such as Wnt and PI3K-Akt[36,62]. In addition, 3D culture-derived exosomes also exhibited enriched protein content responsible for endocytosis and cellular uptake, such as AHSG[12], which may facilitate enhanced intracellular delivery of bioactive cargo. In particular, a study has reported that 3D culture-derived exosomes exhibited unique proteomic profiles, including WNT5A and TGFβ, related to chemotaxis and homing properties that were absent in those from 2D cultures[62]. This distinct molecular composition suggests that 3D culture-derived exosomes may activate key signaling pathways, such as Wnt/β-catenin and TGFβ/Smad, which in turn promote fibroblast migration, proliferation, and viability in vitro[53,59,62]. Considering this notion, further study would be in our best interest to examine the altered protein and nucleic acid profile of exosomes produced using our established potential upscaling protocol compared to the 2D culture-based production.

To better understand the variation observed in the TEM results in this study, we might highlight the experimental setup used in our protocol. In this study phosphate buffer saline (PBS) was used to store exosomes, as a recommended buffer to maintain exosome integrity[63]. Furthermore, PBS is considered safe and compatible with clinical standards, ensuring the clinical application of our exosome preparation. However, the usage of PBS buffer upon the TEM sample preparation may introduce salt deposition, interfering with the staining process.

Furthermore, a contrasting technique using uranyl acetate was used during the TEM sample preparation to enhance visualization. Negative staining using uranyl acetate for TEM imaging is a common technique aimed at enhancing the contrast for visualization of exosome morphology. However, uranyl salts may form a complex with phosphate ions, leading to precipitate formation and uneven staining quality. This issue may be correlating to the great variation in exosome morphology imaging with high background as observed in this study. It correlates to the previous study in which visible salt deposits generated low contrast and high background in TEM images, interfering with the recognition of vesicle morphology[64].

According to the variation observed in the gap closure rate result, the following clarification should be noted. In this study, the in vitro wound healing assay was conducted by maintaining fibroblast cultures in serum-free DMEM as the basal medium, omitting the co-founding effect of serum supplementation. Moreover, to evaluate the cell migration and behavior throughout the incubation period, the gap closure rate was assessed over three distinct time intervals: 0–12 h, 12–24 h, and the overall 0–24 h period. This calculation was performed using linear regression, in which the wound gap area was plotted against the designated incubation time. Hence, the slope derived from the regression equation served as the gap closure rate.

A great variation was observed in the gap closure rate of negative control in the VSCBIC-3-2D group, marked by an outlier in the dataset during the 12–24 h incubation time. This data point is likely associated with the minimum slope generated from the equation, further indicating the low migration rate of the particular replicate during the later stage of incubation. This result is possibly attributed to the behavior of the cells upon prolonged serum deprivation.

Our finding aligns with the previous study reported that serum deprivation prompted the defect in NIH3T3 fibroblast migration due to the failure in trailing edge retraction necessary for cell movement. High variation of the data set of cell phenotype, and protrusive activity was also reported upon 12–16 h of serum starvation[65]. This may reflect the challenge for cells to adapt to the nutrient-deficient environment, leading to less predictable and high variation migration activity in the subsequent stages of the assay.

This study was aimed at establishing the fundamental platform for the production of exosome product for clinical application. To set up the principal platforms, the study's objectives were set up in two major parts, the first is to establish the "potential upscaling protocol" for producing exosomes from cAD-MSCs. Secondly, exploration of the potential application of the cAD-MSCs-derived exosomes produced from the "potential upscaling protocol" for wound healing in vitro.

For the establishment of the "potential upscaling protocol" for the production of cAD-MSC-derived exosomes. The practical upscaling protocol was conducted by using a 3D culture system with microcarrier-assisted culture along with the use of an in-house serum-free exosome collecting medium (VSCBIC-3). This was to ensure that the upscaling protocol was feasible for further pre-industrial-scale production and had the freedom to operate (FTO) according to the patented intellectual property.

In this regard, the evaluation assays used for confirming the upscaling protocol efficiency needed to be complied with an international standards and regulatory guidelines to make it feasible for further registration process with the regional and national drug control authorities. In this study, we preliminarily referred to the recommendations by the International Society for Extracellular Vesicles (ISEV) as detailed in the MISEV2018[44] and MISEV2023[45].

According to these guidelines, exosomes should be characterized to determine their abundance by evaluating total particle number and/or protein content. Although the quantification of these components does not perfectly correlate with exosome numbers, it is suggested as a proxy for exosome quantification. The analysis to justify the quantification method, such as the protein-to-particle ratio, was recommended to indicate the degree of purity. In addition to the quantification of bulk exosome preparation, single vesicle analysis allows for the visualization of individual exosomes, providing information related to their structure and morphology for ensuring the purity of exosome components.

The aforementioned approach has been widely used in preceding research to evaluate and compare exosomes produced from different protocols[12,33,39,42,63]. The comparison of parameters including exosome morphology, expression of exosome-specific surface markers, particle size and distribution, particle-to-protein ratio, and zeta potential were used to reflect the exosome qualitatively. Furthermore, exosome productivity comparison was based on quantitative parameters such as the exosome yield and concentration in a conditioned medium.

In the next phase of the study, we plan to further investigate the components of cAD-MSC-derived exosomes produced by our upscaling protocol by using the bioinformatics and multi-omics approaches to define the potential active molecules governing the biological activities.

To explore the potential application of the cAD-MSCs-derived exosomes produced from the potential upscaling protocol for wound healing, phenotypic and genotypic analyses were employed. This information provided the potential benefits of the exosomes and suggested the potential aspects of further in vivo study models. Based on our upscaling production protocol, the in-house serum-free exosome collecting medium (VSCBIC-3) along with the exosome collecting process using TFF were used to ensure the quality and purity of exosome components. By this method, the exosome components in this product were mainly derived from cAD-MSCs' secretion, not from the FBS. Our established exosome collection protocol aimed to avoid the isolation of exosomes and soluble particles derived from the serum. This approach ensures the purity of exosome preparation, providing reliable results portraying exosomes' utmost efficacy.

To study the phenotypic properties of cAD-MSC-derived exosomes on wound healing properties, fibroblast-based wound healing assays were conducted. According to the fibroblast-based wound healing assays, it is worth highlighting that fibroblasts are one of the key cell populations governing wound healing, involved in multiple stages of the healing process, prominently during proliferation and matrix remodeling stages. Fibroblast migration and proliferation in the wound site are the key to granulation tissue formation, and further, play a pivotal role in regulating collagen deposition and releasing various soluble mediators essential for extracellular matrix remodeling. In this study, fibroblast-based proliferation and wound-healing (in vitro migration) assays along with the artificial intelligence assistance were used for determining the phenotypic properties of cAD-MSC-derived exosomes on wound healing properties. Further genotypic properties were explored to see the dynamic of mRNA marker expression relating to wound healing and help suggested the potential underlying mechanism governing the phenotypic phenomena.

It is also important to note that this study involves the discovery and development of exosome-based wound treatment potential, in addition to the in vitro preclinical study exploring cAD-MSCs-derived exosome wound healing activity on fibroblast. This research marks the initial step of the drug development process, corresponding to step 1 and 2 as defined by the United States Food and Drug Administration (US FDA)[66]. These promising results lay the groundwork for subsequent research phases. Moving forward, our study further aims to advance to subsequent stages for this development, which may involve in vivo pre-clinical studies, and ultimately step 3 regarding clinical trials.

In summary, it is evident that the established potential upscaling protocol allowed the enhanced exosome production and bioactivity of cAD-MSC-exosomes. This protocol establishment involves the establishment of an exosome-collecting medium and microcarrier-based 3D-culture system. Our comparative analysis exhibits the enhanced effect of cAD-MSC-exosomes produced by this platform on fibroblast in vitro, suggesting potential wound treatment.

Methods

Ethical approval and guidelines

The study protocol was approved by the Institutional Animal Care and Use Committee (IACUC) of the Faculty of Veterinary Science, Chulalongkorn University (Animal Use Protocol No. 2231041). In addition, all experiments were performed in accordance with the Animal Research: Reporting of In Vivo Experiments (ARRIVE) guidelines; the International Society for Cellular Therapy (ISCT) Guidance[15]; the Minimal information for studies of extracellular vesicles (MISEV) 2018[44] and 2023[45] by the International Society for Extracellular Vesicles (ISEV).

Isolation and culture of cAD-MSCs

The procedures were performed following the approved guidelines and regulations by the Institutional Animal Care and Use Committee (IACUC) of the Faculty of Veterinary Science, Chulalongkorn University (Animal Use Protocol No. 2231041). The cAD-MSCs were isolated and cultured in accordance with our previous studies[16,17]. In brief, adipose tissue samples were collected under anesthesia from the abdominal fat of each donor ($n=4$). The donor inclusion criteria included healthy dogs aged between 10 months and 5 years, weighing over 5 kg, and the participation was contingent upon the owner's consent. The tissue was washed with Phosphate Buffer Saline (PBS, Thermo Fisher Scientific) containing 2% Antibiotic–Antimycotic (Thermo Fisher Scientific), followed by mincing and incubating within Cell Recovery Solution (Corning) for 2 h at 37 °C. The mixture was subsequently filtered through a 70 µm Falcon™ Cell Strainers (Corning), followed by washing using PBS and centrifuged at 600 g for 5 min, twice repeatedly. The collected cells were resuspended and seeded onto a 100 mm-culture dish (Corning) utilizing routine used growth medium consisting of Dulbecco's Modified Eagle Medium (DMEM, Thermo Fisher Scientific), 10% fetal bovine serum (FBS, Thermo Fisher Scientific), 1% GlutaMAX™ (Thermo Fisher Scientific), and 1% Antibiotic–Antimycotic (Thermo Fisher Scientific) at 37 °C in a humidified incubator with 5% CO_2.

Characterization of of cAD-MSCs

The cAD-MSCs were characterized according to The International Society for Cellular Therapy (ISCT) Guidance[15] through assessing cell morphology, surface marker expression, stemness, and proliferation marker expression, and multilineage differentiation potency. Cell morphology was examined under a phase-contrast microscope (EVOS™ Core Imaging System microscope; Thermo Fisher Scientific). The mRNA expressions related to stemness makers (*Rex1* and *Oct4*) and proliferative marker (*Ki67*) were analysed by means of reverse transcription-quantitative polymerase chain reaction (RT-qPCR). Surface marker expression related to MSCs (CD73, CD90, CD29, and CD44) and hematopoietic cells (CD45) was examined by flow cytometry. Staining was performed using specific antibodies, namely PE-conjugated mouse anti-human CD29 monoclonal antibody (BioLegend), PE-conjugated rat anti-dog CD90 monoclonal antibody (eBioscience), Alexa Fluor 488-conjugated rat anti-dog CD44 antibody (BioRad), mouse anti-human CD73 monoclonal antibody (Thermo Fisher Scientific) and FITC-conjugated goat anti-mouse immunoglobulin G (IgG) as the secondary antibody (BioRad), FITC-conjugated mouse anti-human CD45 monoclonal antibody (BioLegend). While isotype controls used in this study were PE-conjugated mouse IgG1 kappa Isotype (BioLegend), PE-conjugated rat IgG2b kappa Isotype (eBioscience), Alexa Fluor 488-conjugated rat IgG2a Isotype (BioRad), FITC-conjugated mouse IgG1 kappa Isotype (BioLegend), mouse IgG2a kappa Isotype (Thermo Fisher Scientific). The analysis was performed using the BD FACSCalibur Flow Cytometer (BD Bioscience).

The multilineage differentiation potency of cAD-MSCs was assessed using adipogenic, osteogenic, and chondrogenic small molecules induction protocols based on previous studies[18,67]. Osteogenic differentiation protocol commenced by seeding 2.5×10^4 cells onto 24-well culture plate, followed by maintenance using osteogenic induction medium containing routine used growth medium supplemented with 50 mg/mL ascorbic acid (Sigma), 100 mM dexamethasone (Sigma), and 10 mM β-glycerophosphate (Sigma) for 14 days. The mineralization of ECM was detected using Alizarin Red staining (Sigma). The expression of osteogenic-related markers, i.e., *Runx2, Osx* and *Ocn* was examined using RT-qPCR.

For the chondrogenic differentiation protocol, cells were seeded on 24-well plates (Corning) within 5×10^4 cell/well density and maintained in a chondrogenic induction medium containing DMEM (Thermo Fisher Scientific) supplemented with 15% FBS (Thermo Fisher Scientific), 1% GlutaMAX™ (Thermo Fisher Scientific), 1% Antibiotic–Antimycotic, 50 mg/mL ascorbic acid (Sigma), 4 mg/ml L-proline (Sigma), 0.1 µM dexamethasone (Sigma), 1% insulin-transferrin-selenium (ITS, Thermo Fisher Scientific), and 10 ng/mL transforming growth factor beta 3 (TGF-β3, Sigma). The formation of glycosaminoglycan was analyzed using Alcian Blue staining (Sigma) after 21 days of maintenance. The mRNA expression of chondrogenic-related markers (*Sox9* and *Col2a1*) was assessed using RT-qPCR.

Briefly, the adipogenic differentiation protocol was conducted for 28 days. Cells were seeded on 24-well plates (Corning) within 3×10^4 cell/well density and maintained in adipogenic induction medium containing growth medium supplemented with 1 µM dexamethasone (Sigma), 0.2 mM indomethacin (Sigma), 1 mM 3-isobutyl-1-methylxanthine (IBMX, Sigma), and 0.1 mg/mL insulin (Sigma-Aldrich) for 72 h, followed by 24 h maintenance in adipogenic maintenance medium consist of growth medium supplemented with 0.1 mg/mL insulin. Those induction cycles were subjected to up to 5 cycles following maintenance until 28 days in total. Finally, the generated intracellular lipid droplets were detected using Oil Red O staining (Sigma), and the expression of adipogenic-related markers, i.e. *Leptin* and *LPL* was examined using RT-qPCR.

Preparation of in-house exosome-collecting medium

The basal medium, SF-DMEM, utilized in this study consisted of DMEM supplemented 1% GlutaMAX™ (Thermo Fisher Scientific), and 1% Antibiotic–Antimycotic (Thermo Fisher Scientific) which was also used as a group

comparison to the established in-house media. Various exosome-collecting media were chemically defined and tailored based on our prior unpublished investigation. These modifications included different supplementation of the basal medium as follows: (i) exosome-depleted-FBS supplemented medium (dEx-DMEM), consisting of basal medium supplemented with 5% of in-house exosome-depleted-FBS, (ii) in-house exosome-collecting solution (VSCBIC-3), consisted of basal medium modified by the addition of chemically defined supplements in which the exact formulation cannot be disclosed due to the confidential contract, (iii) exosome-depleted-FBS supplemented in-house exosome-collecting solution (dEx-VSCBIC-3), consist of in-house VSCBIC-3 solution supplemented with 5% of in-house exosome-depleted-FBS. Meanwhile, a routine growth medium was used as a control in this study.

Resazurin and live/dead assay

After maintaining cAD-MSCs in various exosome-collecting media, cell population was analyzed using resazurin assay at days 1, 2, 3, and 4. Briefly, the cell was incubated in a medium containing 0.015 mg/mL resazurin (Sigma) for 3 h, the absorbance was then measured using a spectrophotometer at wavelengths of 570 nm and 600 nm. The percentage of resazurin reduction was calculated according to a previous study[68].

The qualitative analysis of cell viability was assessed using live/dead double staining at 1, 2, 3, and 4 days of incubation. The cells were washed with sterile PBS and incubated in a serum-free medium containing 1 µg/mL calcein-AM and 1 µg/mL propidium iodide for 20 min. The evaluation was performed using a confocal microscope system (AX / AX R with NSPARC, Nikon).

Exosome production: conventional 2D culture

Two production protocols based on conventional 2D culture were established and evaluated in this study: (i) SF-DMEM-2D, utilizing SF-DMEM as the exosome-collecting medium, which also served as a control, (ii) VSCBIC-3-3D, utilizing VSCBIC-3 as the collecting medium. In brief, cAD-MSCs were seeded into tissue culture dish and allowed to adhere for 24 h, the growth medium was then replaced with the exosome-collecting medium. The cells were maintained in their respective exosome-collecting media for 48 h, during which the conditioned medium was collected every 24 h. Conditioned medium from 24-hour and 48-hour time points was pooled and filtered through a 0.22 µm sterile syringe filter unit (Thermo Fisher Scientific) to remove larger particles, such as debris, cells, and apoptotic bodies. Subsequently, exosomes were isolated in accordance with previous studies[43,69] using an ultrafiltration system by filtering conditioned medium using Amicon Ultra-4 100 kDa centrifugal filter unit (Merck) which was centrifuged at 5000 g for 20 min. The concentrate was collected and subsequently diafiltrated using PBS (Sigma), and eventually filtered through a 0.22 µm sterile syringe filter unit (Thermo Fisher Scientific). The isolated exosomes were then stored at -80 °C for further experiments.

Exosome production: microcarrier-based 3D culture

A potential upscaling protocol, VSCBIC-3-3D, was developed using microcarrier-based 3D culture and VSCBIC-3 as the exosome-collecting medium, referring to previous studies[12,70]. Initially, Enhanced Attachment Microcarriers (Corning) was hydrated within the growth medium containing DMEM supplemented with 10% FBS (Thermo Fisher Scientific), 1% Antibiotic-Antimycotic (Thermo Fisher Scientific), and 1% GlutaMAX™ (Thermo Fisher Scientific) for 2 h at 37 °C in 250 mL spinner flask (Corning). cAD-MSCs was seeded within the system according to the seeding protocol which involved intermittent agitation lasting for 24 h. Once cells were attached and homogenously spread throughout the microcarrier, cell conditioning was conducted by replacing the growth medium with VSCBIC-3, exosome-collecting solution, followed by maintenance for 48 h. The conditioned medium was harvested after conditioning for 24 h by collecting 75% of the total medium. The conditioned medium was further filtered through a 0.22 µm sterile syringe filter unit (Thermo Fisher Scientific). In accordance with previous experiments[12,43] exosomes were isolated through the TFF system by using Pellicon® XL50 with Biomax® 100 kDa Membrane (Merck), followed by diafiltration using PBS (Thermo Fisher Scientific). Finally, exosomes were filtered through a 0.22 µm sterile syringe filter unit (Thermo Fisher Scientific) and stored at -80 °C for further experiment.

Exosome characterization

Exosome characteristics were examined referring to Minimal information for studies of extracellular vesicles (MISEV2023)[45]. Particle size and distribution were measured by Nanoparticle Tracking Analysis using NanoSight NS300 (Malvern). In summary, the sample was injected using an automatic syringe pump (Malvern), and video was recorded for each sample within five replicates at camera level 14 for 1 min ($n=4$). The generated data was analyzed using NanoSight NTA 3.2 software[12,43,71]. Exosomal protein was measured using AccuOrange™ protein quantification kit (Biotium) according to its manufacturer's instruction[71]. Exosome morphology was illustrated using a transmission electron microscope JEM-1400 (JEOL). In a brief, 10uL of exosomes sample was pipetted onto a copper grid and incubated for 5 min. The excess liquid was then removed by blotting. The grid was further incubated with 2% uranyl acetate for 2 min, and the excess liquid was removed by blotting[64]. Flow cytometry analysis was conducted to detect the expression of the CD9 exosomal surface marker. Briefly, aliquoted sample ($n=3$) of exosomes (100uL) was stained using ExoBrite™ CD9 Flow Antibody (Biotium) according to the manufacturer's instructions, and the expression was detected using CytoFLEX LX Nanoscale Flow Cytometer (Beckman Coulter). For zeta potential measurement, the exosomes sample was diluted 1:20 in PBS. Afterward, the zeta potential was measured in 3 replicates *using* Zetasizer Nano ZSP (Malvern), and the acquired data was analyzed using Zetasizer 7.4 software[72].

Migration assay

3T3-J2 fibroblasts was seeded in a 24-well plate at a density of 5×10^4 cells/well and incubated at 37 °C until reaching a monolayer confluency. Subsequently, a scratch was generated at the center of each well using SPLScar™ Scratcher (SPL Life Science) and washed with PBS (Sigma) to eliminate debris. The cells were then co-cultured with exosomes produced from various protocols (at concentrations of 10^6, 10^7, 5×10^7, and 10^8 particle/mL), while cells maintained in serum-free basal medium was served as untreated control. The gap closure process was observed at multiple time points (0, 6, 12, 18, and 24 h) using a brightfield microscope (confocal microscope system AX / AX R with NSPARC, Nikon). Subsequently, closure rate analysis and comparisons were conducted using NIS-Elements Advanced Research (Nikon).

Proliferation assay

For the one-day proliferation assay, 3T3-J2 fibroblasts were seeded on 96-well plate within 5×10^3 cells per well density and allowed to adhere for 24 h. The cells were then co-cultured with VSCBIC-3-3D-exosomes at concentrations of 10^6, 10^7, 5×10^7, and 10^8 particle/mL for 24 h, while cells cultured in serum-free basal medium was subjected as untreated control group. Resazurin assay was performed by adding a solution of resazurin (Sigma) to each well until reaching a final concentration of 0.015 mg/mL within the medium, followed by 3 hours incubation. The absorbance was measured using a spectrophotometer at wavelengths of 570 nm and 600 nm.

Meanwhile, to examine the long-term effect of exosome therapy, serial time point proliferation assay was carried out. Addressing cells' serum dependency issue, DMEM supplemented with 3.5% FBS (Sigma) served as the basal medium and untreated control group. Briefly, 3T3 fibroblasts were co-cultured with or without VSCBIC-3-3D-exosomes at various concentrations, followed by resazurin assay at day 1, 2, 3, and 4 to evaluate cell proliferation.

Reverse transcription-quantitative polymerase chain reaction

Total RNA was extracted using TRIzol® reagent (Invitrogen) and Direct-Zol RNA isolation kit (ZymoResearch), followed by RNA conversion to complementary DNA (cDNA) using Improm-II™ Reverse Transcription System kit (Promega) according to the manufacturer's protocol. Quantitative real-time PCR was subsequently using PowerUp™ SYBR™ Green Master Mix Kit (Thermo Fisher Scientific) and specific primers through Bio-Rad Real-Time PCR Detection System (Bio-Rad). The primer utilized in this study was summarized in Supplementary Table S1. The mRNA expression was normalized using Glyceraldehyde 3-phosphate dehydrogenase (*Gapdh*) for canine cells and ribosomal Protein L13 (*Rlp13A*) for mouse cells. Relative mRNA value was calculated using the $2^{-\Delta\Delta t}$ method by comparing it to the control group.

Statistical analysis

The generated data was plotted and statistically analysed using RStudio (Posit Software, version 2023.06.1 + 524) and presented as mean and standard deviation (mean ± SD). Kruskal Wallis test was used to compare more than two groups of samples, meanwhile, Man-Whitney U test was utilized for pairwise comparisons between two groups. In addition, the correlation between two different variables was calculated using Pearson's correlation coefficients. The p-value < 0.05 was considered statistically significant.

Data availability

The datasets used and/or analyzed during the current study available from the corresponding author on reasonable request.

Received: 29 March 2024; Accepted: 5 March 2025
Published online: 27 March 2025

References

1. Prasai, A., Jay, J. W., Jupiter, D. & Wolf, S. E. El Ayadi, A. Role of exosomes in dermal wound healing: A systematic review. *J. Invest. Dermatology*. **142**, 662–678e668. https://doi.org/10.1016/j.jid.2021.07.167 (2022).
2. Ayavoo, T., Murugesan, K. & Gnanasekaran, A. Roles and mechanisms of stem cell in wound healing. *Stem Cell. Investig.* **8**, 4. https://doi.org/10.21037/sci-2020-027 (2021).
3. Zeng, Q. L. & Liu, D. W. Mesenchymal stem cell-derived exosomes: an emerging therapeutic strategy for normal and chronic wound healing. *World J. Clin. Cases.* **9**, 6218–6233. https://doi.org/10.12998/wjcc.v9.i22.6218 (2021).
4. Dai, W. et al. Microenvironmental cue-regulated exosomes as therapeutic strategies for improving chronic wound healing. *NPG Asia Mater.* **14** https://doi.org/10.1038/s41427-022-00419-y (2022).
5. Vu, N. B. et al. Stem cell-derived exosomes for wound healing: current status and promising directions. *Minerva Med.* **112**, 384–400. https://doi.org/10.23736/s0026-4806.20.07205-5 (2021).
6. Katsha, A. M. et al. Paracrine factors of multipotent stromal cells ameliorate lung injury in an Elastase-induced emphysema model. *Mol. Ther.* **19**, 196–203. https://doi.org/10.1038/mt.2010.192 (2011).
7. Li, D. & Wu, N. Mechanism and application of exosomes in the wound healing process in diabetes mellitus. *Diabetes Res. Clin. Pract.* **187**, 109882. https://doi.org/10.1016/j.diabres.2022.109882 (2022).
8. He, X. et al. MSC-Derived Exosome Promotes M2 Polarization and Enhances Cutaneous Wound Healing. *Stem Cells Int* 7132708, (2019). https://doi.org/10.1155/2019/7132708 (2019).
9. Gupta, D., Zickler, A. M. & El Andaloussi, S. Dosing extracellular vesicles. *Adv. Drug Deliv. Rev.* **178**, 113961. https://doi.org/10.1016/j.addr.2021.113961 (2021).
10. Cao, J. et al. Three-dimensional culture of MSCs produces exosomes with improved yield and enhanced therapeutic efficacy for cisplatin-induced acute kidney injury. *Stem Cell. Res. Ther.* **11**, 206. https://doi.org/10.1186/s13287-020-01719-2 (2020).
11. Rezaie, J., Feghhi, M. & Etemadi, T. A review on exosomes application in clinical trials: perspective, questions, and challenges. *Cell. Commun. Signal.* **20**, 145. https://doi.org/10.1186/s12964-022-00959-4 (2022).
12. Haraszti, R. A. et al. Exosomes produced from 3D cultures of MSCs by tangential flow filtration show higher yield and improved activity. *Mol. Ther.* **26**, 2838–2847. https://doi.org/10.1016/j.ymthe.2018.09.015 (2018).

13. Casajuana Ester, M. & Day, R. M. Production and utility of extracellular vesicles with 3D culture methods. *Pharmaceutics* **15** https://doi.org/10.3390/pharmaceutics15020663 (2023).
14. Jonkman, J. E. N. et al. An introduction to the wound healing assay using live-cell microscopy. *Cell Adhes. Migr.* **8**, 440–451. https://doi.org/10.4161/cam.36224 (2014).
15. Dominici, M. et al. Minimal criteria for defining multipotent mesenchymal stromal cells. The international society for cellular therapy position statement. *Cytotherapy* **8**, 315–317. https://doi.org/10.1080/14653240600855905 (2006).
16. Dang Le, Q. et al. In vitro generation of transplantable insulin-producing cells from canine adipose-derived mesenchymal stem cells. *Sci. Rep.* **12**, 9127. https://doi.org/10.1038/s41598-022-13114-3 (2022).
17. Rodprasert, W. et al. Tailored generation of insulin producing cells from canine mesenchymal stem cells derived from bone marrow and adipose tissue. *Sci. Rep.* **11**, 12409. https://doi.org/10.1038/s41598-021-91774-3 (2021).
18. Nantavisai, S. et al. Systems biology analysis of osteogenic differentiation behavior by canine mesenchymal stem cells derived from bone marrow and dental pulp. *Sci. Rep.* **10**, 20703. https://doi.org/10.1038/s41598-020-77656-0 (2020).
19. Ivanovska, A. et al. Immunophenotypical characterization of canine mesenchymal stem cells from perivisceral and subcutaneous adipose tissue by a species-specific panel of antibodies. *Res. Vet. Sci.* **114**, 51–58. https://doi.org/10.1016/j.rvsc.2017.02.019 (2017).
20. Kim, H. R. et al. Extensive characterization of feline intra-abdominal adipose-derived mesenchymal stem cells. *J. Vet. Sci.* **18**, 299–306 (2017).
21. Humenik, F. et al. A comparative study of canine mesenchymal stem cells isolated from different sources. *Anim. (Basel).* **12** https://doi.org/10.3390/ani12121502 (2022).
22. Purbantoro, S. D., Osathanon, T., Nantavisai, S. & Sawangmake, C. Osteogenic growth peptide enhances osteogenic differentiation of human periodontal ligament stem cells. *Heliyon* **8**, e09936. https://doi.org/10.1016/j.heliyon.2022.e09936 (2022).
23. Davies, R. et al. Extracellular vesicle depletion protocols of foetal bovine serum influence umbilical cord mesenchymal stromal cell phenotype, Immunomodulation, and particle release. *Int. J. Mol. Sci.* **24**, 9242. https://doi.org/10.3390/ijms24119242 (2023).
24. Li, J. et al. Serum-free culture alters the quantity and protein composition of neuroblastoma-derived extracellular vesicles. *J. Extracell. Vesicles*. **4**, 26883. https://doi.org/10.3402/jev.v4.26883 (2015).
25. Giannasi, C. et al. Serum starvation affects mitochondrial metabolism of adipose-derived stem/stromal cells. *Cytotherapy* **25**, 704–711. https://doi.org/10.1016/j.jcyt.2023.03.004 (2023).
26. Man, K., Eisenstein, N. M., Hoey, D. A. & Cox, S. C. Bioengineering extracellular vesicles: smart nanomaterials for bone regeneration. *J. Nanobiotechnol.* **21**, 137. https://doi.org/10.1186/s12951-023-01895-2 (2023).
27. Koh, B. et al. A Three-Dimensional Xeno-Free Culture Condition for Wharton's Jelly-Mesenchymal Stem Cells: The Pros and Cons. *Int. J. Mol. Sci.* **24** https://doi.org/10.3390/ijms24043745 (2023).
28. Ferrari, C. et al. Limiting cell aggregation during mesenchymal stem cell expansion on microcarriers. *Biotechnol. Prog.* **28**, 780–787. https://doi.org/10.1002/btpr.1527 (2012).
29. Takahashi, I., Sato, K., Mera, H., Wakitani, S. & Takagi, M. Effects of agitation rate on aggregation during beads-to-beads subcultivation of microcarrier culture of human mesenchymal stem cells. *Cytotechnology* **69**, 503–509. https://doi.org/10.1007/s10616-016-9999-5 (2017).
30. Hanga, M. P. et al. Scale-up of an intensified bioprocess for the expansion of bovine adipose-derived stem cells (bASCs) in stirred tank bioreactors. *Biotechnol. Bioeng.* **118**, 3175–3186. https://doi.org/10.1002/bit.27842 (2021).
31. Syromiatnikova, V., Prokopeva, A. & Gomzikova, M. Methods of the Large-Scale production of extracellular vesicles. *Int. J. Mol. Sci.* **23** https://doi.org/10.3390/ijms231810522 (2022).
32. Paolini, L. et al. Large-scale production of extracellular vesicles: report on the massivevs ISEV workshop. *J. Extracell. Biology*. **1**, e63. https://doi.org/10.1002/jex2.63 (2022).
33. de Fuzeta, A. Scalable production of human mesenchymal stromal Cell-Derived extracellular vesicles under Serum-/Xeno-Free conditions in a Microcarrier-Based bioreactor culture system. *Front. Cell. Dev. Biol.* **8**, 553444. https://doi.org/10.3389/fcell.2020.553444 (2020).
34. Koh, B. et al. Three dimensional microcarrier system in mesenchymal stem cell culture: a systematic review. *Cell. Biosci.* **10**, 75. https://doi.org/10.1186/s13578-020-00438-8 (2020).
35. Jeske, R. et al. Upscaling human mesenchymal stromal cell production in a novel vertical-wheel bioreactor enhances extracellular vesicle secretion and cargo profile. *Bioactive Mater.* **25**, 732–747. https://doi.org/10.1016/j.bioactmat.2022.07.004 (2023).
36. Muok, L. et al. Extracellular vesicle biogenesis of three-dimensional human pluripotent stem cells in a novel Vertical-Wheel bioreactor. *J. Extracell. Biology*. **3**, e133. https://doi.org/10.1002/jex2.133 (2024).
37. Debbi, L., Guo, S., Safina, D. & Levenberg, S. Boosting extracellular vesicle secretion. *Biotechnol. Adv.* **59**, 107983. https://doi.org/10.1016/j.biotechadv.2022.107983 (2022).
38. Yuan, X. et al. Engineering extracellular vesicles by three-dimensional dynamic culture of human mesenchymal stem cells. *J. Extracell. Vesicles*. **11**, e12235. https://doi.org/10.1002/jev2.12235 (2022).
39. Busatto, S. et al. Tangential flow filtration for highly efficient concentration of extracellular vesicles from large volumes of fluid. *Cells* **7** https://doi.org/10.3390/cells7120273 (2018).
40. Patel, D. B. et al. Impact of cell culture parameters on production and vascularization bioactivity of mesenchymal stem cell-derived extracellular vesicles. *Bioeng. Transl Med.* **2**, 170–179. https://doi.org/10.1002/btm2.10065 (2017).
41. Barekzai, J. et al. Process development for the production of mesenchymal stromal cell-derived extracellular vesicles in conventional 2D systems. *Cytotherapy* **26**, 999–1012. https://doi.org/10.1016/j.jcyt.2024.04.071 (2024).
42. Bader, J., Narayanan, H., Arosio, P. & Leroux, J. C. Improving extracellular vesicles production through a bayesian optimization-based experimental design. *Eur. J. Pharm. Biopharm.* **182**, 103–114. https://doi.org/10.1016/j.ejpb.2022.12.004 (2023).
43. Kim, J. Y. et al. Defined MSC exosome with high yield and purity to improve regenerative activity. *J. Tissue Eng.* **12**, 20417314211008626. https://doi.org/10.1177/20417314211008626 (2021).
44. Thery, C. et al. Minimal information for studies of extracellular vesicles 2018 (MISEV2018): a position statement of the international society for extracellular vesicles and update of the MISEV2014 guidelines. *J. Extracell. Vesicles*. **7**, 1535750. https://doi.org/10.1080/20013078.2018.1535750 (2018).
45. Welsh, J. A. et al. Minimal information for studies of extracellular vesicles (MISEV2023): from basic to advanced approaches. *J. Extracell. Vesicles*. **13**, e12404. https://doi.org/10.1002/jev2.12404 (2024).
46. Ciftci, E. et al. Comparative analysis of magnetically activated cell sorting and ultracentrifugation methods for exosome isolation. *PLoS One*. **18**, e0282238. https://doi.org/10.1371/journal.pone.0282238 (2023).
47. Furuta, T. et al. Mesenchymal stem Cell-Derived exosomes promote fracture healing in a mouse model. *Stem Cells Transl Med.* **5**, 1620–1630. https://doi.org/10.5966/sctm.2015-0285 (2016).
48. Hu, L. et al. Exosomes derived from human adipose mensenchymal stem cells accelerates cutaneous wound healing via optimizing the characteristics of fibroblasts. *Sci. Rep.* **6**, 32993. https://doi.org/10.1038/srep32993 (2016).
49. Oh, E. J. et al. Extracellular vesicles derived from fibroblasts promote wound healing by optimizing fibroblast and endothelial cellular functions. *STEM CELLS*. **39**, 266–279. https://doi.org/10.1002/stem.3310 (2021).
50. Barrientos, S., Brem, H., Stojadinovic, O. & Tomic-Canic, M. Clinical application of growth factors and cytokines in wound healing. *Wound Repair. Regen.* **22**, 569–578. https://doi.org/10.1111/wrr.12205 (2014).
51. Gilbert, R. W. D., Vickaryous, M. K. & Viloria-Petit, A. M. Signalling by transforming growth factor Beta isoforms in wound healing and tissue regeneration. *J. Dev. Biol.* **4** https://doi.org/10.3390/jdb4020021 (2016).

52. Wang, L. et al. Exosomes secreted by human adipose mesenchymal stem cells promote scarless cutaneous repair by regulating extracellular matrix remodelling. *Sci. Rep.* **7**, 13321. https://doi.org/10.1038/s41598-017-12919-x (2017).
53. Jiang, T., Wang, Z. & Sun, J. Human bone marrow mesenchymal stem cell-derived exosomes stimulate cutaneous wound healing mediates through TGF-beta/Smad signaling pathway. *Stem Cell. Res. Ther.* **11**, 198. https://doi.org/10.1186/s13287-020-01723-6 (2020).
54. Battegay, E. J., Raines, E. W., Colbert, T. & Ross, R. TNF-alpha stimulation of fibroblast proliferation. Dependence on platelet-derived growth factor (PDGF) secretion and alteration of PDGF receptor expression. *J. Immunol.* **154**, 6040–6047 (1995).
55. Ritsu, M. et al. Critical role of tumor necrosis factor-α in the early process of wound healing in skin. *J. Dermatology Dermatol. Surg.* **21**, 14–19. https://doi.org/10.1016/j.jdds.2016.09.001 (2017).
56. Chen, X. & Thibeault, S. L. Role of tumor necrosis factor-alpha in wound repair in human vocal fold fibroblasts. *Laryngoscope* **120**, 1819–1825. https://doi.org/10.1002/lary.21037 (2010).
57. Oh, S., Kim, H., Nam, K. & Shin, I. Glut1 promotes cell proliferation, migration and invasion by regulating epidermal growth factor receptor and integrin signaling in triple-negative breast cancer cells. *BMB Rep.* **50**, 132–137. https://doi.org/10.5483/bmbrep.2017.50.3.189 (2017).
58. Kawai-Harada, Y., Nimmagadda, V. & Harada, M. Scalable isolation of surface-engineered extracellular vesicles and separation of free proteins via tangential flow filtration and size exclusion chromatography (TFF-SEC). *BMC Methods*. **1** https://doi.org/10.1186/s44330-024-00009-0 (2024).
59. Faruqu, F. N., Liam-Or, R., Zhou, S., Nip, R. & Al-Jamal, K. T. Defined serum-free three-dimensional culture of umbilical cord-derived mesenchymal stem cells yields exosomes that promote fibroblast proliferation and migration in vitro. *Faseb J.* **35**, e21206. https://doi.org/10.1096/fj.202001768RR (2021).
60. Kim, H. et al. Comprehensive molecular profiles of functionally effective MSC-Derived extracellular vesicles in Immunomodulation. *Mol. Ther.* **28**, 1628–1644. https://doi.org/10.1016/j.ymthe.2020.04.020 (2020).
61. Jarmalaviciute, A., Tunaitis, V., Pivoraite, U., Venalis, A. & Pivoriunas, A. Exosomes from dental pulp stem cells rescue human dopaminergic neurons from 6-hydroxy-dopamine-induced apoptosis. *Cytotherapy* **17**, 932–939. https://doi.org/10.1016/j.jcyt.2014.07.013 (2015).
62. Camoes, S. P. et al. 3D-MSCs A151 ODN-loaded exosomes are Immunomodulatory and reveal a proteomic cargo that sustains wound resolution. *J. Adv. Res.* **41**, 113–128. https://doi.org/10.1016/j.jare.2022.01.013 (2022).
63. Cheng, K. & Kalluri, R. Guidelines for clinical translation and commercialization of extracellular vesicles and exosomes based therapeutics. *Extracell. Vesicle*. **2**, 100029. https://doi.org/10.1016/j.vesic.2023.100029 (2023).
64. Rikkert, L. G., Nieuwland, R., Terstappen, L. & Coumans, F. A. W. Quality of extracellular vesicle images by transmission electron microscopy is operator and protocol dependent. *J. Extracell. Vesicles*. **8**, 1555419. https://doi.org/10.1080/20013078.2018.1555419 (2019).
65. Iwanicki, M. et al. PDZ-RhoGEF and ROCKII cooperate to regulate adhesion movement and trailing-edge Retraction in fibroblasts. *J. Cell Sci.* **121**, 895–905. https://doi.org/10.1242/jcs.020941 (2008).
66. U.S. Food and Drug Administration. *The Drug Development Process*, (2018). https://www.fda.gov/patients/learn-about-drug-and-device-approvals/drug-development-process
67. Purwaningrum, M., Giachelli, C. M., Osathanon, T., Rattanapuchpong, S. & Sawangmake, C. Dissecting specific Wnt components governing osteogenic differentiation potential by human periodontal ligament stem cells through interleukin-6. *Sci. Rep.* **13**, 9055. https://doi.org/10.1038/s41598-023-35569-8 (2023).
68. Mouville, C. & Benaroudj, N. Vol. 2134 215–228 (2020).
69. Zhang, J. et al. Exosomes derived from human endothelial progenitor cells accelerate cutaneous wound healing by promoting angiogenesis through Erk1/2 signaling. *Int. J. Biol. Sci.* **12**, 1472–1487. https://doi.org/10.7150/ijbs.15514 (2016).
70. Jeske, R. et al. Agitation in a Microcarrier-based spinner flask bioreactor modulates homeostasis of human mesenchymal stem cells. *Biochem. Eng. J.* **168** https://doi.org/10.1016/j.bej.2021.107947 (2021).
71. Kim, M. K., Choi, Y. C., Cho, S. H., Choi, J. S. & Cho, Y. W. The antioxidant effect of small extracellular vesicles derived from Aloe vera peels for wound healing. *Tissue Eng. Regen Med.* **18**, 561–571. https://doi.org/10.1007/s13770-021-00367-8 (2021).
72. Midekessa, G. et al. Zeta potential of extracellular vesicles: toward Understanding the attributes that determine colloidal stability. *ACS Omega*. **5**, 16701–16710. https://doi.org/10.1021/acsomega.0c01582 (2020).

Acknowledgements

Y.V.P. was supported by Chulalongkorn University's Graduate Scholarship Program for ASEAN or Non -ASEAN Countries, and the 90th Anniversary Chulalongkorn University Fund. In addition, this research is funded by Thailand Science Research and Innovation Fund Chulalongkorn University. The authors thank Ms. Daneeya Chaikiawkeaw (BSc, MSc, PhD), Center of Excellence for Regenerative Dentistry, Faculty of Dentistry, Chulalongkorn University for providing access to spectrofluorometer instrument; and the Center of Excellence for Veterinary Clinical Stem Cells and Bioengineering, Chulalongkorn University for allowing access to the research facility.

Author contributions

Y.V.P. designed and performed the majority of the experiments; collected, analyzed, and interpreted the data; and wrote the manuscript. S.O. and W.R. provided the ideas and designed the exosome production protocols. I.P. provided the research material. N.S. and R.M. provided the analysis and interpretation of data. T.O., P.S., and T.P. supported and provided ideas, C.T. provided substantial revision to the manuscript, C.S. conceived the main ideas; designed the experiments; analyzed and interpreted the data; and wrote and revised the manuscript. All authors have reviewed the manuscript.

Declarations

Competing interests

The authors declare no competing interests.

Additional information

Supplementary Information The online version contains supplementary material available at https://doi.org/10.1038/s41598-025-93219-7.

Correspondence and requests for materials should be addressed to C.S.